Circuits and Systems
Mekelweg 4,
2628 CD Delft
The Netherlands
http://ens.ewi.tudelft.nl/

CAS-2019-03

M.Sc. Thesis

Investigation on Time-of-Arrival Estimation for the LoRa Network

Ming DAI

Abstract

LoRa (Long Range) is a low-power, long-range and low-cost wireless communication system that can facilitate a wide variety of infrastructures for the Internet of Things (IoT). Current algorithms to locate LoRa tags have a resolution of 100 m in practice, and a question is if that can be improved without changing the tags or adding too much to the gateways (basestations).

Conventional delay estimation ranging algorithms extract useful information from the channel frequency response and use this information to estimate delays. In this thesis, three localization techniques are presented: the matched filter, FBCM-MUSIC and TLS-ESPRIT algorithms. Then a multiband architecture is proposed and integrated into the matched filter. These algorithms are implemented in the LoRa system model. The simulations indicate that FBCM-MUSIC and TLS-ESPRIT have better performance than the matched filter in NLOS channels. The results also show that TLS-ESPRIT is more effective and robust compared to MUSIC. The proposed multiband architecture can improve the resolution of TOA estimation and decreases the 90th percentile error by around 40%.

Investigation on Time-of-Arrival Estimation for the LoRa Network

Thesis

submitted in partial fulfillment of the
requirements for the degree of

Master of Science

in

Electrical Engineering

by

Ming DAI
born in Hengshui, China

This work was performed in:

Circuits and Systems Group
Department of Microelectronics & Computer Engineering
Faculty of Electrical Engineering, Mathematics
Delft University of Technology

The work presented in this Master thesis was supported in part by Koninklijke PTT Nederland N.V. (KPN).

Delft University of Technology
Department of
Microelectronics & Computer Engineering

The undersigned hereby certify that they have read and recommend to the Faculty of Electrical Engineering, Mathematics for acceptance a thesis entitled **"Investigation on Time-of-Arrival Estimation for the LoRa Network "** by **Ming DAI** in partial fulfillment of the requirements for the degree of **Master of Science**.

Dated: 26 March 2019

Chairman: _____
Prof.dr.ir. A.J. van der Veen

Advisors: _____
Dr.ir. G.J.M. Janssen

_____
Dr.ir. Z. Irahhauten

Committee Members: _____
Dr. P. Pawelczak

Daily Supervisor: _____
MSc T. Kazaz

Abstract

LoRa (Long Range) is a low-power, long-range and low-cost wireless communication system that can facilitate a wide variety of infrastructures for the Internet of Things (IoT). Current algorithms to locate LoRa tags have a resolution of 100 m in practice, and a question is if that can be improved without changing the tags or adding too much to the gateways (basestations).

Conventional delay estimation ranging algorithms extract useful information from the channel frequency response and use this information to estimate delays. In this thesis, three localization techniques are presented: the matched filter, FBCM-MUSIC and TLS-ESPRIT algorithms. Then a multiband architecture is proposed and integrated into the matched filter. These algorithms are implemented in the LoRa system model. The simulations indicate that FBCM-MUSIC and TLS-ESPRIT have better performance than the matched filter in NLOS channels. The results also show that TLS-ESPRIT is more effective and robust compared to MUSIC. The proposed multiband architecture can improve the resolution of TOA estimation and decreases the 90th percentile error by around 40%.

Acknowledgments

First of all, I would like to express my deep gratitude to all the people who have offered me great help in this master project. They are all affable and easy going.

I would like to thank my supervisor, prof.dr.ir. A.J. van der Veen, for his general guidance to keep me on the track in this thesis process. Also his personal charisma makes me to be more inspired and motivated.

I also want to express my gratitude to supervisor, dr.ir. G.J.M. Janssen, for his valuable assistance during the writing of this thesis. I am much more enlightened thanks to his insight and expertise in this project.

I am grateful to dr.ir. Z. Irahhauten, my supervisor at KPN, for offering me an opportunity to do this thesis project work in KPN. He gives us all support and guidance so that I can complete this project duly. He is patient and responsible in his guidance, although he is with his corporate affairs.

I would like to show my greatest gratitude to my daily supervisor, MSc T. Kazaz, for providing much invaluable guidelines throughout numerous consultations. He spent lots of time looking for related materials and checking the correctness of my work. His consistently supportive and encouraging words kept me motivated and helped build my self-confidence. Tarik, thank you for your time and patience in supervising me over this ten months.

I also want to thank Bart Hendriks, the former project manger at KPN, for his support and project management. He gave me much useful advice on life.

I want to acknowledge KPN for providing the financial support during my thesis project. Thanks to all my friends who were and are in the CAS lab room, for their friendship and companionship. Thank to people who have made valuable comments on my paper which inspire me improve the quality of the thesis. I would like to thank Yefeng CAI, for making me feel less disconnected.

Finally, I would like to thank my family, especially my grandparents, for their immense love and constant encouragement. It was their emotional and financial support that I got the chance to pursuit higher level education in Netherlands.

Ming DAI
Delft, The Netherlands
26 March 2019

Contents

List of Figures

List of Tables

Glossary

AWGN Additive White Gaussian Noise

BW Bandwidth

CDF Cumulative Distribution Function

CIR Channel Impulse Response

CFR Channel Frequency Response

CRLB Cramér–Rao Lower Bound

CSS Chirp Spread Spectrum

CTFT Continuous Time Fourier Transform

DFT Discrete Fourier Transform

DTFT Discrete Time Fourier Transform

EVD Eigenvalue Decomposition

ESPRIT Estimation of Signal Parameters by Rotational Invariance Techniques

LoRa Long Range

LOS Line of Sight

MUSIC Multiple Signal Classification

NLOS Non Line of Sight

PSD Power Spectral Density

RMSE Root Mean Square Error

RSSI Received Signal Strength Indication

SF Spreading Factor

SNR Signal to Noise ratio

TDOA Time Difference of Arrival

TOA Time of Arrival

1 Introduction

1.1 Introduction to LoRa and Geolocation

In recent years, wireless communication system has become an integral part of our daily life. A variety of wireless communication technologies have been invented and it has become one of the most important mediums for information transmission between devices. Different technologies are developed to have more potential in different applications, for example Bluetooth, WiFi and Zigbee, where the former is the best used in short range M2M wireless communication; and the latter two are more suitable for a network of nodes. LoRa (Long Range) is a low-power, long-range and low-cost wireless communication system. To be more specific, LoRa is a radio frequency (RF) transmission technique that allows devices to transmit information over a long distance consuming a very small amount of power. Semtech acquired this technology in 2012 [1] and begun to manufacture LoRa chips and devices. LoRa network comprises of two distinct layers which will be introduced later and for now they are: 1. a physical layer (LoRaPHY) using a patented spread spectrum modulation technique and 2. a MAC layer (LoRaWAN) [2] identifying a specific access network architecture.

LoRaWAN enables GPS-free tracking applications and the infrastructure-based localisation for low-power and wide-area networks. LoRa has the scalability to facilitate a wide variety of infrastructures for the Internet of Things (IoT) [3]. One noticeable feature is that these infrastructures provide a LoRaWAN geolocation solution. LoRaWAN geolocation is a novel approach to locate local devices equipped with LoRaWAN sensors outdoors. It is particularly well suited for static assets which do not require super accurate locations but where an estimate error of 50m is enough. The localisation methods implemented in LoRaWAN protocol can be classified into two categories: Received Signal Strength Indication (RSSI) and Time Difference of Arrival (TDOA). The former one provides a coarse estimation ranging from 1000m to 2000 meters. By contrast, TDOA decreases estimation error to hundreds meters [4], and this finer accuracy makes LoRaWAN a prominent solution to localisation, especially for the applications with a low budget and battery-powered end-devices. The objective of this thesis is to improve the accuracy of TDOA in LoRaWAN protocol.

Next we will explain the advantages of LoRa in outdoor localisation with respect to LoRaPHY and LoRaWAN.

- *Long range and Low power* For most radio communications, it is difficult to transmit signals at a long distance with limited transmission power. Chirp spread spectrum (CSS) modulation [5] that will be explained in chapter 2 enables these long range transmission with limited power. This modulation technique provides significant link budget improvement over conventional narrowband modulation. Most spectrum spreading technologies work above the noise floor to make sure

the successful reception. The enhanced robustness provided by CSS allows LoRa receiver to have a higher sensitivity and receive the signal below the noise floor. Thus the transmission range is extended by LoRa for a fixed power.

- *Tolerance to interference* In wireless communications, interference occurs when some unwanted signals with similar frequencies are added disruptively to the desired signal. The interference degrades the fidelity of the receiver's estimate of the desired received signal. As a spectrum spreading technology, CSS modulation employs six spreading factors. LoRa signals of different spreading factors are orthogonal to each other and thus less susceptible to the interference.
- *Low cost and Long battery life* The well-known satellite-based radio positioning system, GPS, provides the most accurate real-time location updates among all existing technologies. Nonetheless, GPS receivers in end-devices are expensive and exceed the power budget. Other short radio approaches like WiFi and Bluetooth also entail high installation cost on access points and beacon nodes. Comparatively speaking, LoRaWAN has lower deployment requirements and thus cost less.

Before explaining how LoRaWAN geolocation works, I will introduce three important components in LoRaWAN: the end-devices, the gateways and the network server.

- *End-device*: low-power consumption devices with bidirectional wireless communication various sensing abilities. Once the useful information is collected by the certain built-in sensors, it is transferred to the LoRa transceiver to be transmitted to the gateways.
- *Gateway*: a intermediate powerful device that relays packets between end-devices and a network server. The number of gateways in a LoRa deployment is not limited, and the same data packet can be received by more than one gateway simultaneously.
- *Network server*: responsible for processing packets received from multiple gateways, directing them to an application server.

With this basic knowledge of LoRaWAN, we can move on to the principles of LoRaWAN geolocation. A LoRa signal from an end-device is received simultaneously by no less than three nearby gateways whose locations are known in advance, and an accurate timestamp is recorded at the gateway once this transmission arrives. These timestamps are then forwarded to the network server where the position of that end-device will be calculated. Only an uplink transmission is required and not needed to be specific for geolocation. Also TDOA requires perfect synchronisation among gateways which is much easier than the synchronisation between the gateway and the end-device.

1.2 Motivation of thesis work

Two main factors that degrade the accuracy of timestamps are a narrow bandwidth and multipath propagation. In the presence of multipath, arrival paths are not resolvable with 125kHz bandwidth and the estimation only gives an average channel delay.

Given the LoRa signal bandwidth of 125kHz, the distance between two delays has to be larger than $8\mu s$ (2400m) to be distinguished. Some LoRa products are currently able to provide a finer timestamp resolution of 1μs [6]. Within the time duration of 1μs, a radio signal propagates around 300m in air. The estimation resolution of 300m is much better than 2400m but still cannot reach our requirements. As we have mentioned before, we do not require LoRaWAN Geolocation to achieve the same high accuracy as GPS with the constraints of hardware and software. However, we can still refine on the estimation method to bring this estimation resolution below 300m.

The multipath-induced fading is a more general but still troublesome issue when it concerns the wireless communication. LoRa signals from different paths arrive at gateways at different times and are added either constructively or destructively. It is this uncertainty that aggravates the estimation problem. In urban areas, the second or third arriving signal carries the strongest power because the energy of the first arrival signal is attenuated strongly by the buildings. Since correlation based technologies select the strongest part of received signal as the arrival time, it again introduces unpredictable errors.

As we can see, obstacles are ahead and it is not a trivial task to locate end-device positions.

1.3 Problem statement

This project aims to solve two problems:

1. How to implement high-resolution TOA estimation algorithms in the LoRa system to improve the accuracy of timestamps in multipath environment?

2. What is sensitivity of these algorithms to different factors like noise, interference, NOLS propagation and etc.?

1.4 Thesis outline

The thesis is organised as follows:

In chapter 1, a brief background of LoRa and TOA-based localisation is introduced.

In chapter 2, a system model is presented which consists of the transmitted signal model, the channel model and the received signal model.

In chapter 3, at first, a correlation-based technology (the matched filter) is introduced which is a convolution with a time-reversed and conjugated version of the signal. The matched filter is a conventional technique for estimating the signal delays. However, this method is not entirely suitable for the multipath channel model, because its time resolution is limited by the bandwidth. For this reason, two super-resolution algorithms: FBCM-MUSIC and TLS-ESPRIT are introduced with the aim of resolving closely-spaced paths. MUSIC is a subspace-based TOA estimation method which splits the vector space into a signal subspace and a noise subspace. It utilises the orthogonality between these two subspace to estimate the delays. The exact prior knowledge of the number of multipaths is required so that MUSIC is able to have best performance. FBCM-MUSIC is an improved version for the case where only one set of experimental

data is available. ESPRIT exploits the shift invariant structure in the spectrum of the signals. TLS-ESPRIT improves the conventional ESPRIT by constraining wide observing spaces into a single subspace.

In chapter 4, a multiband architecture is proposed to overcome the problem of insufficient bandwidth resources. The basic idea is to estimate the coarse CFR of each band and concatenate them together to achieve a fine estimate.

In chapter 5, the CRLB is derived in detail for the single path scenario.

In chapter 6, the three algorithms are implemented under different scenarios and the simulation results are presented.

2 System Model

In this chapter, we introduce the transmitted signal model, the channel model and at last the received signal model. The signal model is based on the chirp spread modulation and in accordance with the specifications of the LoRa physical layer. The received signal is the convolution of the transmitted signal and the channel.

2.1 Background

As the preamble to the formal introduction of system model, this section presents CSS modulation.

Spread spectrum is a technique referring to the practice of spreading the transmitted signal to the whole frequency spectrum which is used for transmission. A chirp represents a 'Compressed High Intensity Radar Pulse'. It is a complex valued signal whose frequency continuously increases or decreases at a fixed rate. Illustrations of an up-chirp and down-chirp are shown in Fig 2.1. Compared to other spread spectrum schemes, this frequency variation makes the LoRa signal to be more resistant to the interference and achieve a longer communication range .

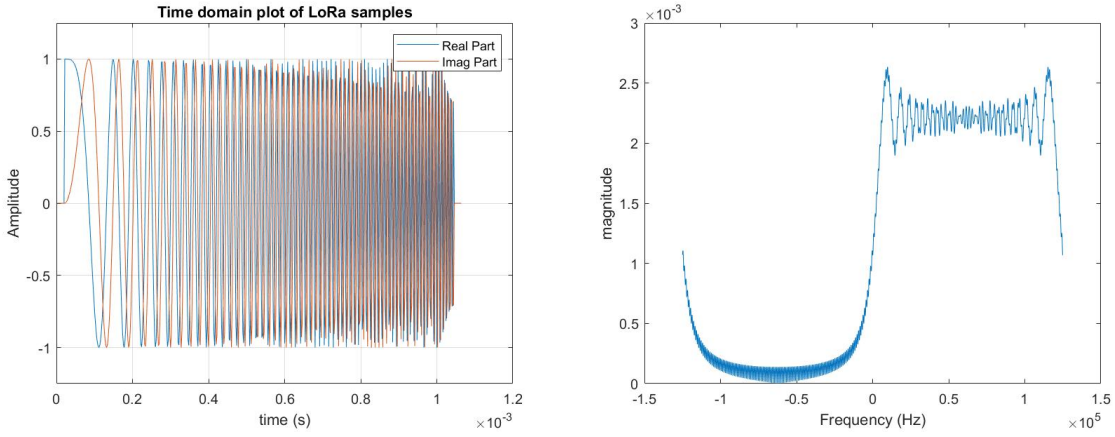

(a) (b)

Figure 2.1: Illustration of an up-chirp in a) time and b) frequency domain used in the LoRa modulation.

It is easy to notice that the power is not uniformly distributed over the desired frequency range. There are some Fresnel ripples in the spectrum of the chirp signal, especially towards the ends of the spectrum. They arise due to the sudden discontinuities in the chirp waveform at the commencement and termination of the pulses.

Two important parameters concerning the CSS modulation are: Bandwidth (BW) and Spreading Factor (SF). LoRa provides three standard bandwidths: 125kHz, 250kHz and 500kHz, and six spreading factor values: 7,8,9,10,11 and 12. Some external factors like battery life, range and transmission power vary from region to region. Therefore, these modulation parameters should be assigned properly to ensure successful reception.

To avoid confusion, the definition of a chip, a symbol and a chirp is given below.

- A chip is the basic binary element in the sequence of data. One chip is sent per second per Hz of bandwidth [7].
- A symbol/chirp is a signal in which the frequency increases (upchirp) or decreases (downchirp) over the frequency band.

The modem modulates the phase of an oscillator to generate a chirp shown in Fig 2.1. The chip rate R_c defines the number of times per second that the modem adjusts the phase, and it also defines the modulation bandwidth, which is $R_c = BW$. For instance, when the modulation bandwidth is 125kHz, 125000 chips can be transmitted per second, or 1 chip is transmitted every $8\mu s$.

The spreading factor is used to define the number of chips containing in one symbol/chirp. Each symbol contains 2^{SF} chips and the symbol rate R_{sym} is defined as

$$R_{sym} = \frac{R_c}{2^{SF}} = \frac{BW}{2^{SF}} \tag{2.1}$$

and the symbol period T_{sym}, the reciprocal of R_{sym}, is defined as

$$T_{sym} = \frac{1}{R_{sym}} = \frac{2^{SF}}{BW}. \tag{2.2}$$

There are 2^{SF} chips in each symbol, which means each symbol is able to encode SF bits of information. According to the definition, a chip is the basic binary element. Taking SF=7 as an example, in an upchirp, these 2^7 chips are encoded as $[0000000, 0000001, 0000010, 0000011, \ldots, 1111110, 1111111]$. This 128-chip long symbol can by cyclically shifted from 0 to 127 positions, and this cyclical shift N_{shift} carries some extra information.

The decimal numbers corresponding to these 2^{SF} binary elements are $[0, 1, 2, 3, \ldots, 2^{SF} - 1]$. The modulated signal is then [8]

$$\begin{aligned} c(kT_c) &= \frac{1}{\sqrt{2^{SF}}} e^{j2\pi[(N_{shift}+k)_{\mathrm{mod}(2^{SF})}]\frac{kT_c}{T_{sym}}} \\ &= \frac{1}{\sqrt{2^{SF}}} e^{j2\pi[(N_{shift}+k)_{\mathrm{mod}(2^{SF})}]\frac{k}{2^{SF}}} \end{aligned} \tag{2.3}$$

where $k = 0, 1, 2, \ldots, 2^{SF} - 1$ is used as the time index, $0 \leq N_{shift} \leq 2^{SF} - 1$, $T_c = 1/R_c$ is the chip period, and mod stands for modulo operation. The frequency increases linearly with k, and the initial frequency is shifted by N_{shift} from 0.

Table 2.1 displays the periods and rates of a LoRa chirp under different spreading factors.

BW/kHz	SF	Tsym/ms	Rsym/Hz
125	7	1.024	976.56
125	8	2.048	488.28
125	9	4.096	244.14
125	10	8.192	122.07
125	11	16.384	61.04
125	12	32.768	30.52

Table 2.1: Some LoRa symbol periods and rates

The physical frame format of LoRa is designed in compliance with Semtech's specifications. At the physical layer, a LoRa PHY frame starts with a preamble/training sequence. One of the preamble functions is the synchronization. After the preamble, an optional PHY Header follows, where some information such as payload length and the existence of some optional structures is contained. The payload is sent after the header, and the frame is finished with an optional CRC. Fig 2.2 displays the spectrum of LoRa physical layer.

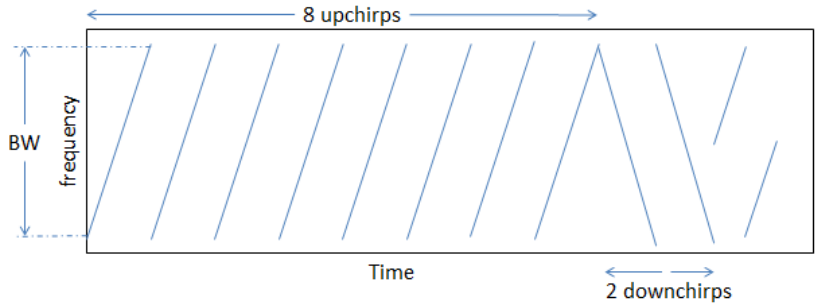

Figure 2.2: The spectrum of LoRa physical layer

2.2 Transmitted signal model

The LoRa signal can be modeled in continuous time as a modulated chirp signal[9]. The chirp signal in (2.3) is simplified to

$$c(t) = e^{j\mu t^2} \qquad (0 < t < T_{sym}) \tag{2.4}$$

where $\mu = (BW)^2/2^{SF}$ [Hz/s], is a constant representing the rate of the instantaneous frequency change of a chirp.

The transmitted LoRa signal can be formulated as

$$s(t) = \sum_{k=0}^{N_{sc}-1} c(t - kT_{sym}) \tag{2.5}$$

where N_{sc} is the number of chirps/symbols.

Fig 2.3 (a) illustrates the real and imaginary part of LoRa signal in time domain and Fig 2.3 (b) shows the spectrum of a standard LoRa packet. The payload transmission starts after the eight-chirp-long preamble and two-chirp-long sync.

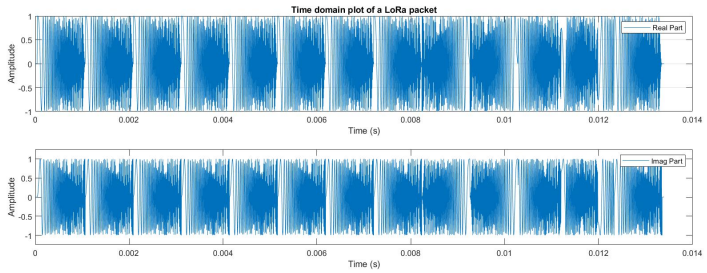

(a)

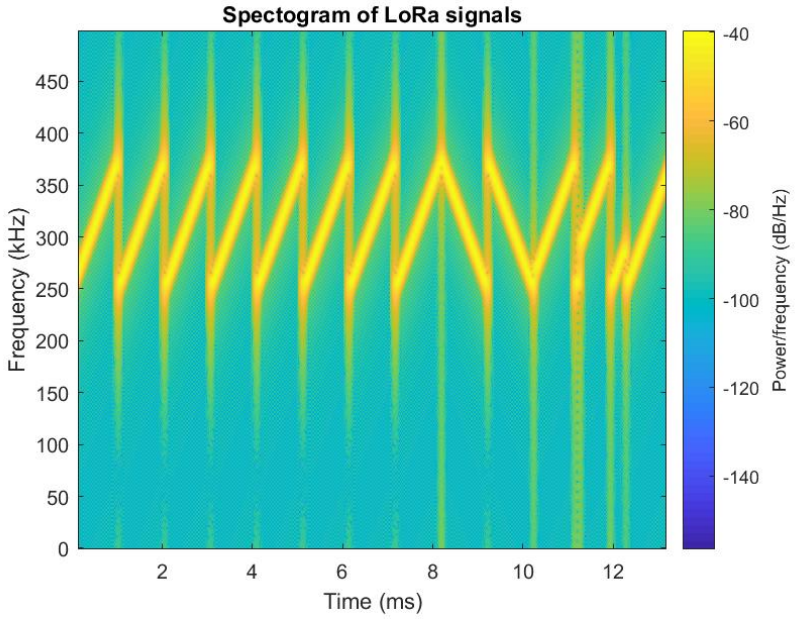

(b)

Figure 2.3: (a) Time domain representation of a LoRa packet (b) spectrogram representation of a standard LoRa packet

2.3 Channel model

The LoRa signal $s(t)$ is sent over a multipath wireless channel, which after demodulation to baseband can be modeled by its impulses responses as

$$h(t) = \sum_{m=0}^{M-1} a_m \delta(t - \tau_m) \tag{2.6}$$

where M is the number of resolvable multipath components, $a_m = g_m e^{-j2\pi f_c \tau_m}$ is complex path attenuation (g_m is the magnitude and $e^{-j2\pi f_c \tau_m}$ represents the phase), τ_m is the propagation delay related to the m-th path and f_c is the central frequency of the carrier on which $s(t)$ is transmitted.

The Continuous Time Fourier Transform (CTFT) of $h(t)$ is

$$H(\Omega) = \int_{-\infty}^{+\infty} h(t) e^{-j\Omega t} dt \tag{2.7}$$

where $\Omega = 2\pi f$, is angular frequency.

The wireless channel consists of a limited number of paths. However, a finite length signal cannot be band-limited. At the receiver, we estimate only a portion of the channel corresponding to $[f_c - BW/2, f_c + BW/2]$. The discrete form of $H(\Omega)$ is needed in the simulation. First, we derive Discrete Time Fourier Transform (DTFT) from CTFT in (2.7):

$$\begin{aligned} H(\Omega) &= \int_{-\infty}^{+\infty} \sum_{n=-\infty}^{n=+\infty} h(nT_s)\delta(t - nT_s) e^{-j\Omega t} dt \\ &= T_s \sum_{n=0}^{N_d - 1} h(nT_s) e^{-j\Omega(nT_s)} \end{aligned} \tag{2.8}$$

$$H(\omega) = \frac{1}{T_s} \sum_{n=0}^{N_d-1} h[n] e^{-j\omega n} = \frac{1}{T_s} \sum_{m=0}^{M-1} a_m e^{-j\omega \frac{\tau_m}{T_s}} \tag{2.9}$$

where $\omega = \Omega T_s$, is the normalized angular frequency, and $|\omega| < 2\pi \frac{BW}{f_s}$. $f_s \geq 2BW$ is the sample rate, $T_s = 1/f_s$ is the sampling period and $N_d = T_{sym}/T_s$, is the number of total samples of one received symbol.

The Discrete Fourier Transform (DFT) should be applied to a finite-duration, discrete-time signal. M in (2.6) is also finite, which means the frequency variables $H[0], H[1], ..., H[N_d - 1]$ in these cases are finite and discrete as well. The discrete expression can be derived from the definition of DFT as

$$H[l] = H(\omega)|_{\omega = \frac{2\pi}{N_d} l} = \frac{1}{T_s} \sum_{m=0}^{M-1} a_m e^{-j\omega_0 \frac{\tau_m}{T_s} l} \quad l = 0, 1, \ldots, N_d - 1 \tag{2.10}$$

where $\omega_0 = \frac{2\pi}{N_d}$.

2.4 Received signal model

2.4.1 Continuous time received signal model

The received baseband signal, after propagation through the multipath wireless channel (2.6), is given by

$$\begin{aligned} x(t) &= \sum_{m=0}^{M-1} a_m s(t-\tau_m) + w(t) \\ &= \sum_{k=0}^{N_{sc}-1} \sum_{m=0}^{M-1} a_m c_k (t - kT_{sym} - \tau_m) + w(t) \end{aligned} \tag{2.11}$$

where $w(t)$ is AWGN with with double-sided power spectral density $N_0/2$ and variance $\sigma^2 = N_0 BW$.

The convolution in time domain corresponds to a multiplication in frequency domain, and it leads to the spectrum of received signal:

$$X(\omega) = \frac{1}{T_s} \sum_{m=0}^{M-1} a_m S(\omega) e^{-j\omega \frac{\tau_m}{T_s}} + W(\omega) \tag{2.12}$$

where $S(\omega)$ is the spectrum of the transmitted signal and $W(\omega)$ is the AWGN noise in frequency domain.

2.4.2 Discrete time received signal model

The received signal is sampled with a sampling rate f_s. The discrete time model for the transmitted and received signal is given by

$$s(nT_s) = \sum_{k=0}^{N_{sc}-1} c(nT_s - kT_{sym}) + w(nT_s) \tag{2.13}$$

$$x(nT_s) = \sum_{m=0}^{M-1} a_m s(nT_s - \tau_m) + w(nT_s) \tag{2.14}$$

where $n = 0, 1, \ldots, N_d - 1$.

The spectrum of the received signal is $R(\omega)$, by following the same transformation steps from $H(\omega)$ to $H[l]$ in chapter 2.3 , the DFT of $r(nT_s)$ is derived as

$$X[l] = \frac{1}{T_s} \sum_{m=0}^{M-1} a_m S[l] e^{-j\omega_0 \frac{\tau_m}{T_s} l} + W[l] \quad l = 0, 1, \ldots, N_d - 1 \tag{2.15}$$

where $S[l]$ and $W[l]$ are the DFT of $s(nT_s)$ and $w(nT_s)$, respectively, $n = 0, 1, \ldots, N_d - 1$ and $\omega_0 = \frac{2\pi}{N_d}$.

3 Algorithms

In this chapter, first a brief overview of the related work is given. Next, four factors regarding TOA estimation techniques are discussed, and they are bandwidth, the noise, complexity and prior knowledge. Finally, we present three TOA estimation algorithms: the Matched Filter, FBCM-MUSIC and TLS-ESPRIT.

For simplicity, the number of symbols N_{sc} is assumed to be 1.

3.1 Background

The LoRa networks use TDOA to locate devices as we have mentioned in chapter 1. The implementation of TDOA can be roughly split into two parts: the timestamp reception at the gateways and the geometric calculation. To attain meter-level ranging accuracy, the order of the timestamping magnitude must be in a nanosecond range. A number of works have been published aiming at analysing LoRa range-based localization and enhancing the estimation accuracy in different scenarios [10, 11, 12, 13, 14].

Based on the timestamps extracted from the received LoRa signals at the gateways, some scientists devised and implemented different TDOA systems [6, 13, 15], which were aimed at higher localization performance. However, these proposals ended with little success. This was because the timestamp resolution only reached a microsecond level.

With respect to the TOA estimation in time domains, two prevailing methods are the maximum likelihood (ML) and the matched filter. The ML estimator [16] requires the prior knowledge of the exact distribution of the multipath. The statistical parameters of the channel vary from one environment to another, and this variance will introduce unpredictable errors to the ML estimator. Another method filters the received signal with a matched filter, and then searches for the maximum of the correlator [17, 18, 19]. Generally, these methods are not complicated and able to carry out good estimates only when the energy of the first arriving component is much stronger than the others, while they attain an inaccurate TOA estimation when this condition is unsatisfied.

Besides, various signal processing approaches have been proposed for the TOA estimation in outdoor environments. The algorithms are known as multiple signal classification (MUSIC) [20, 2], matrix pencil [21], estimation of signal parameters via rotational invariance techniques (ESPRIT) [22, 9, 23] Most of these algorithms process the received signal samples in the frequency domain, where these components are related to the arrival times in time domian as in [24, 25]. High resolution techniques require multiple-experiment data to estimate the correlation matrix with the expectation operation. Nevertheless, sufficient statistically independent channel realizations are not available in many situations.

In non-line-of-sight (NLOS) environments, where a direct path is not observable,

various compensation methods are emerging to mitigate the effect of NLOS errors. Those kinds of NLOS issues are expanded in detail in the literature [26, 27]. Most of the researches aim at estimating TOA of wide-band signals, or multi-subband chirp signals, which are not applicable to a LoRa signal.

The limited bandwidth resources is always a challenge for LoRa radio devices, and many scientists have been working on it over years. Florian et al. [28] created a coherent multi-channel ranging method for narrow-band LoRaWAN and improved the precision bound further in multipath scenarios[29]. The reason behind is that the coherence in multi-channel processing improves the temporal resolution and detection accuracy. In coherent multi-channel ranging, the two-way time-of-flight and phase-of-flight measurement are required to eliminate the phase difference of different channels. The measurement principles work in conjunction with the above mentioned ranging algorithms, and a 200-meter precision is eventually achieved with a 10 kHz signal. Then the author took especially the frequency offsets and multipath influence into account and refined on the Cramer Rao bounds. To utilise more channel resources in this case, two basic premises should be satisfied: 1.a two-way package transmission between the end device and the gateway must be guaranteed. 2.the multi-channel bandwidth should always lie within the radio channel coherence bandwidth. The former is not applicable to all LoRa devices and the latter is not suitable for moving objects.

3.2 Criteria

Before the main content, four factors that affect the performance of these algorithms will be explained in detail: 1.sensitivity to the bandwidth; 2.sensitivity to the signal to noise ratio (SNR) or the noise; 3 the complexity of algorithms; 4.the prior information.

Bandwidth To what extent will the two closely-spaced paths be separated? It is roughly determined by the signal bandwidth. In wireless environments, the signal that arrives at the receiver is a superposition of shifted versions of the transmitted signal due to the channel multipath. This overlapping is a significant error source in the TOA estimation, especially when the multipaths are not resolvable. Only when the delay difference between each two paths is larger than the minimum pulse duration, which is in inverse proportion to the bandwidth, multipaths can be regarded as resolvable. In this case, either lower pulse duration or higher signal bandwidth can mitigate the effects of the multipaths. It is obvious that correlation based techniques are more sensitive to the bandwidth regarding both the resolution and the accuracy of the estimation.

Noise The additive noise is the second major error source apart from the multipath in the TOA estimation. In the single path channel, the accuracy of various techniques is mainly limited by the noise level. The sensitivity to noise can also be interpreted as the robustness of the algorithms. Lower sensitivity to the noise means that the techniques are more robust. Some techniques retain high robustness only when the SNR is above a certain threshold, and the performance becomes more uncontrollable beyond that threshold.

Complexity In most realistic and practical applications, the complexity of the algorithms virtually precedes all the other considerations. From the perspective of industrial design, the best trade-off between the complexity and other factors should be chosen.

The complexity will be the least thing we take into consideration in our project.

Prior knowledge Some algorithms require prior knowledge like a coarse estimation of the path delay, and others need the information of the source signal. Correlation based techniques use the source signal to do correlation and sub-space based techniques estimate the channel frequency response with the help of the source signal.

3.3 Correlation Based Techniques

3.3.1 Matched Filter

The matched filter is virtually a correlation based technique. It performs a temporal match by correlating a template signal with all possible shifts of the received signal $x(t)$. In reality, the transmitted signal is regarded as the optimal template signal to perform the correlation, it is called the matched filter $s_{\mathrm{MF}}(t) = s^*(-t)$. The delays can be estimated by finding the local maxima of the correlation between the matched filter $s_{\mathrm{MF}}(t)$ and the received signal $x(t)$:

$$\begin{aligned} y[n] &= (x * s_{\mathrm{MF}})[n] \\ &= \sum_{m=0}^{M-1} a_m \left(\sum_{k=0}^{N_d-1} s[k - \frac{\tau_m}{T_s}] s^*[k-n] \right) + \sum_{l=0}^{N_d-1} w[l] s^*[l-n] \end{aligned} \tag{3.1}$$

When $n = \frac{\tau_m}{T_s}$, $y[n]$ reaches a maximum. Fig 3.1 illustrates how the matched filter is implemented.

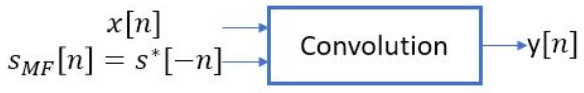

Figure 3.1: Implementation of the Matched Filter

A convolution in time domain is equivalent to a multiplication in frequency domain, the correlation process can be implemented in frequency domain as well. Note that the TOA estimation is more sensitive to the multipath effect than the effect of the additive noise. In other words, the performance of this technique degenerates severely in the multipath channel due to some extra unknown parameters. All the multipath components can be regarded as self interference that will reduce the SNR of the received signal. In addition, it is inaccurate to detect the first arrival path from the highest peak of the result of the matched filter in the NLOS channel.

Compared to other methods, the matched filter is optimal for a single path in noise in terms of the algorithm computational complexity. Moreover, a prior knowledge is not necessary. Although the advantages of the matched filter are obvious, its disadvantages are manifest as well. As we have discussed before, the inability to resolve the closely-spaced multipath components makes it less competitive. Besides the effects of the multipath, the signal bandwidth is another factor that plays an important role in the performance of all correlation-based techniques. The signal bandwidth, or the width of the minimum samples is a main determinant of the resolution of TOA estimation

for the matched filter. In our project, a $125kHz$ bandwidth is used in the outdoor environment and Nyquist sample rate is adopted in the system, the detectable ranging error of LOS signal is around $1.2km$, which is far from the localisation requirements.

3.4 Subspace Based Techniques

Subspace based algorithms decompose the space which is spanned by vectors of channel frequency response (CFR) into several subspaces. Mostly these subspaces consist of a signal subspace and a noise subspace which are orthogonal to each other. Subspace based algorithms utilise this property to estimate various channel parameters. Due to it, they have higher resolution in the parameter estimation. However, the eigenvector decomposition (EVD) of big size matrices cannot be avoided and the complicity makes these techniques less likely to be considered for practical applications.

3.4.1 CFR Estimation

Both MUSIC and ESPRIT require the channel frequency response as the input, and simple approach of CFR estimation will be introduced in this section.

Based on (2.12), the relationship between the spectrum of the transmitted signal and the CFR can be expressed as

$$\mathbf{X} = \mathbf{SH} + \mathbf{W} \tag{3.2}$$

where $\mathbf{X} = [X[0], \ldots, X[N_d-1]]^T$, $\mathbf{S} = \text{diag}(S[0], \ldots, S[N_d-1])$, $\mathbf{H} = [H[0], \ldots, H[N_d-1]]^T$ and $\mathbf{W} = [W[0], \ldots, W(N_d-1)]]^T$. Now we define a new vector $\mathbf{Y} = \mathbf{S}^{-1}\mathbf{X}$, and the frequency range is restricted between $[-BW/2, BW/2]$. Then by replacing the new vector in (3.2), we have

$$\mathbf{Y} = \mathbf{H} + \mathbf{W_{new}} = \mathbf{Va} + \mathbf{W_{new}} \tag{3.3}$$

and its corresponding matrix form:

$$\begin{bmatrix} Y[0] \\ Y[1] \\ \vdots \\ Y[N_d-1] \end{bmatrix} = \begin{bmatrix} 1 & \ldots & 1 \\ \phi(\tau_0) & \ldots & \phi(\tau_{M-1}) \\ \vdots & \ldots & \vdots \\ \phi(\tau_0)^{N_d-1} & \ldots & \phi(\tau_{M-1})^{N_d-1} \end{bmatrix} \begin{bmatrix} a_0 \\ a_1 \\ \vdots \\ a_{M-1} \end{bmatrix} + \begin{bmatrix} W[0] \\ W[1] \\ \vdots \\ W[N_d-1] \end{bmatrix} \tag{3.4}$$

where $\mathbf{W_{new}} = \mathbf{S}^{-1}\mathbf{W}$ represents the additive noise in vector $\mathbf{Y}$ and $\phi(\tau) = e^{-j\frac{2\pi}{N_d}\frac{\tau}{T_s}}$. Note that the noise enhancement is inevitable when dividing $X[l]$ by $S[l]$, it should be taken carefully at low signal levels. In the following, $\mathbf{W_{new}}$ and $\mathbf{W}$ are used interchangeably for simplicity. N_d is defined in (2.9) as T_{sym}/T_s, or its equivalent form $2^{SF}/(T_s\text{BW})$.

3.4.2 FBCM-MUISC

MUSIC, a super-resolution algorithm, is based on the eigenvalue-decomposition (EVD) of the autocorrelation matrix of the signal model. It was first used for azimuth estimation and later applied to TOA estimation. MUSIC aims to exactly exploit the underlying information of the signals that hides behind the noise. FBCM-MUSIC is an improvement of conventional MUSIC providing better resolution.

The autocorrelation matrix is defined as

$$\mathbf{R}_Y = E\{\mathbf{Y}\mathbf{Y}^H\} = \mathbf{V}\mathbf{A}\mathbf{V}^H + \sigma_w^2\mathbf{I} \tag{3.5}$$

where $\mathbf{A} = E\{\mathbf{a}\mathbf{a}^H\}$, $\mathbf{I}$ is the $N_d \times N_d$ identity matrix and superscript H stands for the conjugate transpose of a matrix. The matrix $\mathbf{V}$ has full column rank M when τ_m in (2.6) are all different values. As a consequence, the rank of the square matrix $\mathbf{R}_Y$ is also M under the condition $N_d > M$. This means that $N_d - M$ smallest eigenvalues equal to the noise variance σ_w^2. The noise subspace consists of the eigenvectors that correspond to these noise eigenvalues. The rest M largest eigenvalues are signal eigenvalues and the corresponding eigenvectors comprise the signal subspace. The orthogonality between the signal subspace and the noise subspace is the spirit of MUSIC. The projection matrix of the noise subspace is then given by

$$\mathbf{P}_w = \mathbf{Q}_w(\mathbf{Q}_w^H\mathbf{Q}_w)^{-1}\mathbf{Q}_w^H = \mathbf{Q}_w\mathbf{Q}_w^H \tag{3.6}$$

where $\mathbf{Q}_w = [q_M \quad q_{M+1} \quad \dots \quad q_{N_d-1}]$ and $q_k, M \le k \le N_d - 1$, are noise eigenvectors. For a vector that lies in the signal subspace, we have

$$\mathbf{P}_w\mathbf{v}(\tau_m) = 0 \tag{3.7}$$

where $\mathbf{v}(\tau) = [1 \quad \phi(\tau) \quad \phi(\tau)^2 \quad \dots \quad \phi(\tau)^{N_d-1}]^T$. The multipath delays are at the values at which the following MUSIC pseudo-spectrum achieves maximum,

$$P_{MU}(\tau) = \frac{1}{|\mathbf{P}_w\mathbf{v}(\tau)|^2} = \frac{1}{\mathbf{v}^H(\tau)\mathbf{P}_w\mathbf{v}(\tau)} \tag{3.8}$$

Fig 3.3 presents a block diagram of the MUSIC TOA estimation algorithm.

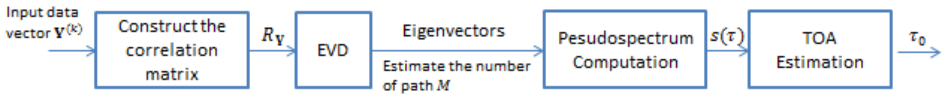

Figure 3.2: Functional flowchart of TOA estimation using MUSIC

In the above analysis, the theoretical correlation matrix $\mathbf{R}_Y$ is considered. In practical implementations, the correlation matrix must be estimated from multiple measurement data samples. Considering that only one set of measurement data is available, the estimation of $\mathbf{R}_Y$ in (3.5) will be reduced to $\mathbf{R}_Y = \mathbf{Y}\mathbf{Y}^H$. Without the expectation operation, the rank of $\mathbf{R}_Y$ is then equal to the rank of $\mathbf{Y}\mathbf{Y}^H$, becomes 1. The lack of full-rank matrix disables the separation between the signal subspace and the noise subspace.

In (3.3), there are M components in $\mathbf{V}$, but only one single vector $\mathbf{Y}$ is used to construct $\mathbf{R}_Y$. In this case, it is not possible to estimate multiple parameters from $\mathbf{R}_Y$. To deal with it, we split $\mathbf{Y}$ into several sub vectors and make a new correlation matrix out of these sub vectors[20]. The sub vector $\mathbf{Y}_k$ is introduced:

$$\mathbf{Y}_k = [Y[k] \quad \dots \quad Y[k+L-1]]^T \tag{3.9}$$

where $M \leq L \leq N_d$.

The new vector $\mathbf{Y}_k$ can be expressed as

$$\mathbf{Y}_k = \mathbf{V}'\mathbf{\Phi}^k\mathbf{a} + \mathbf{W}' \qquad (L \times 1) \tag{3.10}$$

where

$$\mathbf{V}' = \begin{bmatrix} 1 & \dots & 1 \\ \phi(\tau_0) & \dots & \phi(\tau_{M-1}) \\ \vdots & \dots & \vdots \\ \phi(\tau_0)^{L-1} & \dots & \phi(\tau_{M-1})^{L-1} \end{bmatrix}$$

$$\mathbf{\Phi} = \text{diag}(\phi(\tau_0) \quad \phi(\tau_1) \quad \dots \quad \phi(\tau_{M-1}))$$

$$\mathbf{a} = [a_0 \quad a_1 \quad \dots \quad a_{M-1}]^T$$

$$\mathbf{W}' = [W[0] \quad W[1] \quad \dots \quad W[L-1]]^T$$

The new correlation matrix is

$$\hat{\mathbf{R}}_Y = \frac{1}{P}\sum_{k=0}^{P-1}\mathbf{Y}_k\mathbf{Y}_k^H = \mathbf{V}'\mathbf{A}'\mathrm{V}'^H + \sigma_w^2\mathbf{I} \tag{3.11}$$

where $P = N_d - L + 1$, $\mathbf{A}' = \sum_{k=0}^{M-1}(\mathbf{\Phi}^k\mathbf{a}\mathbf{a}^H(\mathbf{\Phi}^k)^H)$ is full rank since the values in the vector $\mathbf{a}$ are assumed to be all different.

A technique named forward-backward linear prediction in [30] is used to ensure that the correlation matrix is conjugate symmetric:

$$\mathbf{R}_Y^{(FB)} = \frac{1}{2}(\hat{\mathbf{R}}_Y + \mathbf{J}\hat{\mathbf{R}}_Y^*\mathbf{J}) \tag{3.12}$$

where $\mathbf{J}$ is the $L \times L$ exchange matrix.

Compared to correlation based techniques, MUSIC is more powerful to separate a finite number of closely-spaced paths. This is because MUSIC utilises the orthogonality between the signal subspace and the noise subspace, and this property makes MUSIC less sensitive to the bandwidth and the noise. However, the increase in both the resolution and the accuracy are at the cost of higher complexity. The complexity that comes from the matrix EV decomposition makes it less competitive in practical applications. In addition, aside from the source signal, MUSIC also requires the number of paths as prior information. As the exact number of paths M is always hard to acquire, then the inaccurate estimated M becomes another error source of MUSIC.

3.4.3 TLS-ESPRIT

MUSIC and ESPRIT are both recognized as classic methods within the scope of spectral estimation. In a way, ESPRIT can be considered as an extension of MUSIC. This algorithm can be split into two steps: 1. reconstruct the matrix of CFR to form an invariance relationship and 2. exploit the underlying rotational invariant structure among the signal subspaces to solve an eigenvalue or singular-value equation. ESPRIT has two variants: the original one and an updated total least squares (TLS) version. The latter has lower bias in the frequency estimates and is used in our project.

The first step is to construct a matrix out of sets of $\mathbf{Y}_k$ as

$$\mathbf{Z} = [\mathbf{Y}_0, \mathbf{Y}_1, \ldots, \mathbf{Y}_{(P-1)}] \quad (L \times P) \tag{3.13}$$

where $\mathbf{Y}_k$ and L are defined in (3.9), and P is defined in (3.11). This reconstruction allows us to estimate a model with multiple components as long as $N_d - P \geq P$. It is a vital condition to be checked, because ESPRIT requires $\mathbf{Z}$ to be a low-rank factorization.

$\mathbf{Z}$ has the model

$$\mathbf{Z} = \mathbf{V}'\mathbf{a}' \tag{3.14}$$

where $\mathbf{a}' = [\mathbf{a} \quad \mathbf{\Phi a} \quad \ldots \quad \mathbf{\Phi}^{P-1}\mathbf{a}]$, $\mathbf{V}'$ and $\mathbf{\Phi}$ are defined in (3.10).

It is evident that each column in $\mathbf{V}'$ has a shift-invariant structure. This model is equipped with a form that can be used by ESPRIT: split the matrix $\mathbf{Z}$ into two sub-matrices $\mathbf{Z}_u$ and $\mathbf{Z}_d$

$$\mathbf{Z} = \begin{bmatrix} \mathbf{Z}_u \\ * * * \end{bmatrix} = \begin{bmatrix} * * * \\ \mathbf{Z}_d \end{bmatrix} \tag{3.15}$$

where $\mathbf{Z}_u$ contains all but the last rows of $\mathbf{Z}$, and $\mathbf{Z}_d$ contains all but the first columns of $\mathbf{Z}$. From the factorization of $\mathbf{Z}$, it is easier to see that

$$\mathbf{Z}_u^{\dagger}\mathbf{Z}_d = \mathbf{T}^{-1}\mathbf{\Phi}\mathbf{T} \tag{3.16}$$

where $\mathbf{T}$ is a $P \times P$ invertible matrix that maps one basis into the other. The eigenvalues of $\mathbf{Z}_u^{\dagger}\mathbf{Z}_d$ correspond to the values of the elements lying on the diagonal of this matrix . Once the values of the diagonal elements of matrix are known, it is possible to find the unknown delays τ_i. So far, the solution has been achieved from the conventional ESPRIT.

TLS ESPRIT is essentially a generalized eigenvalue decomposition based on least squares. It constrains M observing spaces into a single subspace. However, the operator of least square often entails some mathematical problems. The TLS ESPRIT is devised to transform the generalized ill-conditioned problems to small dimension and well conditioned problems. Next, the TLS ESPRIT method will be implemented in the following steps.

- Create $N_d - P - 1 \times 2M$ matrix $\mathbf{O} = [\mathbf{Z}_u \quad \mathbf{Z}_d]$
- Compute its SVD: $\mathbf{O} = \mathbf{U}_o\mathbf{\Sigma}_o\mathbf{V}_o$

- Partition $2M \times 2M$ matrix $\mathbf{V}_o$ to $M \times M$ block matrices as

$$\mathbf{V}_o = \begin{bmatrix} \mathbf{V}_{11} & \mathbf{V}_{12} \\ \mathbf{V}_{21} & \mathbf{V}_{22} \end{bmatrix} \tag{3.17}$$

- TLS-solution is

$$\mathbf{\Phi} = -\mathbf{V}_{12}\mathbf{V}_{22}^{-1} \tag{3.18}$$

After the steps above, the unknown delays are obtained from the eigenvalues of $\mathbf{\Phi}$ and estimated as $\tau = -\text{imag}(\log(\mathbf{\Phi}))\frac{N_d T_s}{2\pi}$.

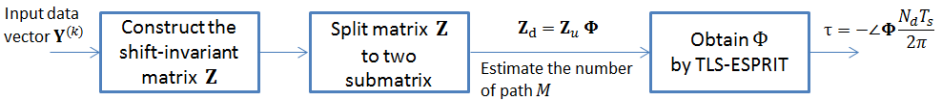

Figure 3.3: Functional flowchart of TOA estimation using TLS ESPRIT

Like MUSIC, the prime thing of ESPRIT aims to make use of more information about the signal. In this case, the source signal and the number of paths present in the measurements should be known as the prior information. If the estimate of the number of path is inaccurate, ESPRIT may perform even worse. TLS ESPRIT manifests considerably lower computational complexity compared to MUSIC. It produces less biased estimates over conventional ESPRIT.

3.5 Comparison of TOA Estimation Tecnhiques

Two types of TOA estimation techniques have been presented in the previous sections. At the beginning of this chapter, four factors related to the algorithms are introduced. Here, we compare the pros and cons of these TOA estimation algorithms with regard to the presented criteria in Tab 3.1.

Table 3.1: Comparison of Delay Estimation Algorithms

	Resolution	Complexity	Note
Matched Filter	Low	Low	No prior information
FBCM-MUSIC	High	High	More specific signal model Fails to resolve closely spaced signals at low SNRs
TLS-ESPRIT	High	High	Less biased estimates Accurate number of path is needed

4 Improvements

There are different bands defined in EU for the LoRaWAN network. Table 4.1 lists out LoRa frequency channels from 863 to 870 MHz [31].

Table 4.1: LoRa ISM frequency bands

Channel Number	LoRa Central Frenquency
CH_10_868	865.20 MHz
CH_11_868	865.50 MHz
CH_12_868	865.80 MHz
CH_13_868	866.10 MHz
CH_14_868	866.40 MHz
CH_15_868	866.70 MHz
CH_16_868	867 MHz
CH_17_868	868 MHz

With the frequency spectrum growing to be a scarce resource, it is vital to utilise the spectrum in a more effective way in the wireless communication system. One possible solution[32] is to use the cognitive radio (CR) system. CR systems are capable of detecting the environment and selecting the available frequency bands. By this means, the spectrum resource is exploited to a higher extent and the interference effects are decreased. Next, we introduce the multiband architecture that will be incorporated in the LoRa TOA system.

4.1 Multiband Ranging Estimation

These channels enable the multiband TOA estimation with higher precision [33]. Restricted by the duty cycle, it is not possible to transmit signals on different bands at the same time. It is necessary to assume that all the transmissions on k bands happen within the coherent time. In other words, the channel remains static during the whole transmission. As specified by LoRa, the separation between the central frequency of two noncontiguous bands is either 0.3MHz or integer multiples of 0.3MHz. In this case, if K bands are used, then (3.2) can be substituted by

$$\mathbf{X}_k = \mathbf{S}_k\mathbf{H}_k + \mathbf{W}_k \tag{4.1}$$

where $\mathbf{X}_k$, $\mathbf{S}_k$, $\mathbf{H}_k$ and $\mathbf{W}_k$, $k \in 0, \ldots, K-1$, are spectrum with length N_d belonging to the kth band. It is obvious that

$$f_{ck} = f_{c0} + 0.3M \times k, \quad k \in 0, \ldots, K-1 \tag{4.2}$$

where f_{ck} is the central frequency of the signal from each single band. As shown in Fig 4.1, different time slots are allocated for the transmission on each band, and a coarse CFR estimation can be easily achieved from each single band. The coarse CFR from each band is then concatenated to achieve a fine TOA estimate. Here we adopt the architecture in [33].

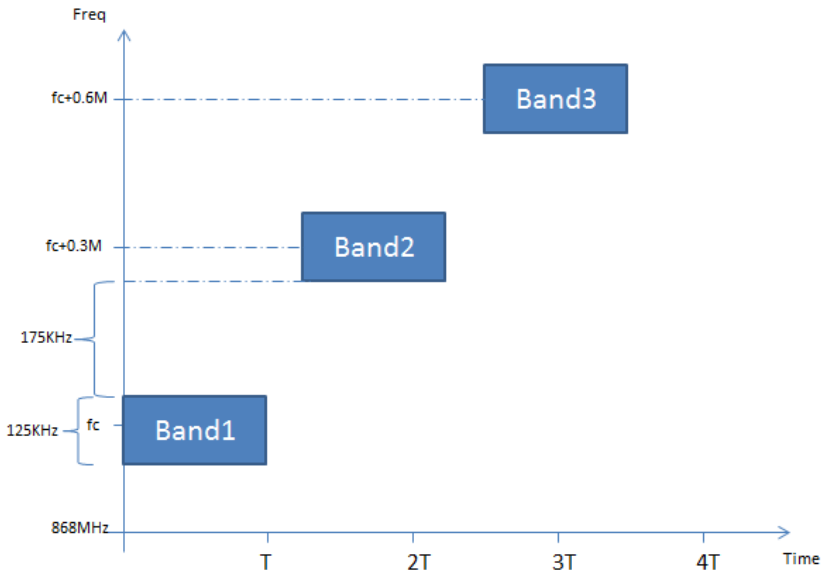

Figure 4.1: Spectrum of transmitted signal with sequential bands

As shown in Fig 4.2, we first shift the whole spectrum by the central frequency f_{ck} to obtain the equivalent complex band pass received signal. Next a band pass filter is applied to remove the noise outside the spectrum $[-\frac{BW}{2} + 0.3M \times k, \frac{BW}{2} + 0.3M \times k]$. After applying the DFT and the inverse filter, a coarse CFR estimate for each band is achieved as $\mathbf{Y}_k$. The equivalent total CFR can be expressed as $\mathcal{Y} = [\mathbf{Y}_0, \mathbf{C}_0, \ldots, \mathbf{C}_{K-2}, \mathbf{Y}_{K-1}]$, where $\mathbf{C}_k$ corresponds to the frequency range over which no signal is transmitted. Since the unavailable bands $\mathbf{C}_k$ do not transmit any signal or carry any information, we fill them with zeros. Then $\mathcal{Y}$ can be rewritten as $\mathcal{Y} = [\mathbf{Y}_0, \ldots, \mathbf{Y}_{K-1}]$.

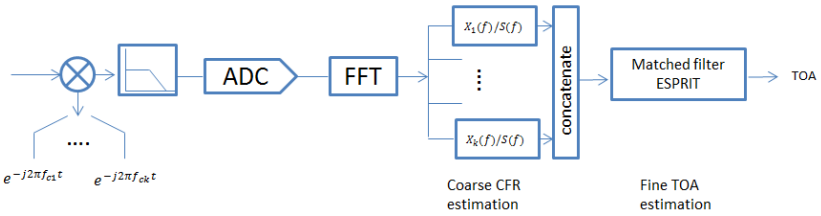

Figure 4.2: Flowchart of the multiband architecture

The multiband architecture, if we put it in another way, it's a bandwidth of $K(BW) + (K-1)(0.3M - BW)$ with some missing information. The effective bandwidth is equal to $K(BW)$ and we concatenate these available bands in a direct way.

The sample rate for the total band is assumed to be equal. The blank frequency band between two sub bands has a bandwidth of $0.3M - BW = 175$kHz and the number of samples for the bandwidth BW is N_d. The vector $\mathcal{Y}$ contains $KN_d + (K-1)(\frac{175k}{125k}N_d)$ samples in total.

In chapter 3, we already introduced three algorithms which are only applied in single-band scenario. Next we discuss how to integrate the multiband structure with range estimation techniques and the feasibility of the proposed architecture.

4.2 Matched Filter with Concatenated Spectrum

Here, we transform the matched filter into frequency, and the single-band correlation result fin frequency domain is

$$\mathbf{Y} = \mathbf{S}^*\mathbf{X} + \mathbf{W} \tag{4.3}$$

where $\mathbf{Y} = [([0], \ldots, Y[N_d-1])^T$, $\mathbf{S} = \text{diag}(S[0], \ldots, S[N_d-1])$, $\mathbf{X} = (X[0], \ldots, X[N_d-1])^T$ and $\mathbf{W} = (W[0], \ldots, W[N_d-1])^T$.

$\mathbf{Y}$ is the CFR from a single band. In this multiband architecture, K sets of $\mathbf{Y}$ are estimated corresponding to the K noncontiguous frequency bands. Then the CIR can be estimated by applying IDFT on $\mathbf{Y}$. According to the definition of CIR, there should be peaks at the time delays in the recovered channel.

At first, the inverse Fourier transform matrix $\mathbf{F}$ is introduced as

$$\mathbf{F}_N = \frac{1}{N}\begin{bmatrix} 1 & 1 & \ldots & 1 \\ 1 & \mathsf{w}_N^1 & \ldots & \mathsf{w}_N^{N-1} \\ \vdots & \ldots & \ldots & \vdots \\ 1 & \mathsf{w}_N^{N-1} & \ldots & \mathsf{w}_N^{(N-1)^2} \end{bmatrix} \tag{4.4}$$

where $\mathsf{w} = e^{j2\pi/(NT_s)}$ and N is the number of IDFT.

Taking the number of bands $K = 2$, and we consider four cases:

$$\begin{aligned}
\mathbf{Y} &= [Y[0] \quad Y[1] \quad \ldots \quad Y[N_d-1]]^T \\
\mathcal{Y}_c &= [Y[0] \quad Y[1] \quad \ldots \quad Y[2N_d-1]]^T \\
\mathcal{Y}_{cz} &= [Y[0] \quad Y[1] \quad \ldots \quad Y[2N_d-1] \quad 0 \quad 0 \quad \ldots]^T \\
\mathcal{Y}_{nc} &= (Y[0] \quad \ldots \quad Y[N_d-1] \quad 0 \quad \ldots \quad 0 \quad Y[N_{cz}-N_d] \quad \ldots \quad Y[N_{cz}-1])^T
\end{aligned}$$

where $\mathcal{Y}_c$ stands for the CFR of wireless channel with two contiguous sub bands, it is a vector with length $2N_d$ corresponding to the two neighboring sub bands. $\mathcal{Y}_{cz}$ extends $\mathcal{Y}_c$ to a length of N_{cz} by zero padding, which corresponds to a bandwidth of $2BW + (0.3M - BW) = (BW + 0.3M)$Hz. $\mathcal{Y}_{nc}$ represents the CFR of wireless channel for two noncontiguous sub bands, it has the same length as $\mathcal{Y}_{cz}$ but all zero elements are shifted after the first N_d elements. These zeros represent the band that is between two sub bands.

The estimation of CIR is given by

$$\hat{h} = \mathbf{F}_{N_d}\mathbf{Y}$$
$$\hat{h}_c = \mathbf{F}_{2N_d}\mathcal{Y}_c$$
$$\hat{h}_{cz} = \mathbf{F}_{3.4N_d}\mathcal{Y}_{cz}$$
$$\hat{h}_{nc} = \mathbf{F}_{3.4N_d}\mathcal{Y}_{nc}$$

where $\hat{h}$, $\hat{h}_c$, $\hat{h}_{cz}$ and $\hat{h}_{nc}$ are the estimated impulse response of the multipath channel corresponding to $\mathbf{Y}$, $\mathcal{Y}_c$, $\mathcal{Y}_{cz}$ and $\mathcal{Y}_{nc}$.

Theoretically, the first arrival delay estimated from $\hat{h}_c$ should be more accurate than that of $\hat{h}$, because more information is provided in $\mathcal{Y}_c$. $\hat{h}_c$ and $\hat{h}_{cz}$ have different lengths but give exactly the same TOA estimates, since the nonzero samples in $\mathcal{Y}_c$ and $\mathcal{Y}_{cz}$ are same. As for $\mathcal{Y}_{nc}$, we could expect a better TOA estimate, since the correlation between two noncontiguous bands is smaller than two contiguous bands. With the same number of samples, a smaller correlation between two bands results in more effective information about the spectrum. In terms of the TOA estimation accuracy that can be provided by the four estimated CIR, the rank of them should be $\hat{h} < \hat{h}_c = \hat{h}_{cz} \leq \hat{h}_{nc}$.

This proposed scheme can be integrated with the matched filter to improve the localisation performance in a multipath environment. As we have proved above, IDFT is able to recover the wireless channel from an incomplete CFR and the missing information has no impact on the TOA estimation. However, this distortion in spectrum disables MUSIC and ESPRIT to perform properly.

4.3 Conclusion

In this chapter, we investigate a way of utilising multi bands to improve the precision of TOA estimation.The signals are transmitted over different frequency spectrum sequentially. The information of both the available narrow bands and unavailable blank spaces are concatenated to increase the accuracy of ranging techniques. Using these non-contiguous bands, we can achieve the same or even better accuracy and resolution as we use the equivalent bandwidth. Note that we incorporate the multiband architecture into the matched filter and ESPRIT instead of MUSIC, because more samples in CFR increase the computational complexity in MUSIC and render it more inefficient.

Two main challenges that prevent the multiband architecture coming into effect are the duty cycle and the phase shift. There is a clash between the duty cycle and the coherent time. Duty Cycle indicates the fraction of time a resource is busy. In the European frequency plan, it has channels in different sub-bands, and the duty cycle should also be considered in this case. The LoRaWAN specification dictates the frequencies of all LoRaWAN-compliant networks for over-the-air activation. In most regions this duty cycle is set to 1% [34]. However, a successful multiband concatenation requires all the transmission to finish within the coherent time. A balance should be drawn between these two factors. Another big issue is the phase shift or carrier frequency offset. It is impossible to synchronize the gateway with the carrier signal contained in the LoRa received signal. The phase difference of the received signals

from two bands may lead to a disaster in the TOA estimation. In our project, we assume the signals from multi bands are in phase. This issue can actually be solved by two-way transmission. Two-way transmission somehow eliminates the phase difference and this will be a promising future to incorporate it into the multiband spectrum ranging estimation.

5 Analysis

5.1 CRLB Derivation

The Cramer-Rao bound (CRB) defines the least amount of variance that unbiased estimators can achieve [35] [36]. In this section, the CRLB is derived for range estimation for LoRa signals based on time of arrival (TOA).

In the single path channel, the received signal model in (2.11) can be simplified to

$$x(t) = s(t-\tau) + w(t) \qquad 0 \le t \le T_{sym} \tag{5.1}$$

The samples in (2.14) are taken every $T_s \ge 1/(2BW)$ to form the discrete data model

$$x(nT_s) = s(nT_s - \tau) + w(nT_s) \qquad n = 0, 1, \ldots, N-1. \tag{5.2}$$

$x[n]$ and $w[n]$ are the sample sequences. $w[n]$ is defined as Gaussian white noise, and it has the variance $\sigma^2 = N_0(BW)$.

The signal s is independent from τ. The probability density function (PDF) of $x[n]$ is

$$p(\mathbf{x};\tau) = \frac{1}{(2\pi\sigma^2)^{\frac{N}{2}}} \exp\left(-\frac{1}{2\sigma^2}\sum_{n=0}^{N-1}(x[n]-s[n])^2\right). \tag{5.3}$$

where $\mathbf{x}$ is a vector collecting the received data samples: $\mathbf{x} = [x[0], x[1], \ldots, x[N_d-1]]$. Two differential operations result in

$$\frac{\partial^2 \ln p(\mathbf{x};\tau)}{\partial\tau^2} = \frac{1}{\sigma^2}\sum_{n=0}^{N-1}\{(x[n]-s[n])\frac{\partial^2 s[n]}{\partial\tau^2} - (\frac{\partial s[n]}{\partial\tau})^2\} \tag{5.4}$$

In this model, the range information depends on the time delay of the received signal. The expected value yields the CRB relative to the delay

$$\begin{aligned} \mathrm{var}(\hat{\tau}) &\ge \mathbf{E}[-\frac{\partial^2}{\partial\tau^2}\ln(p(\mathbf{x};\tau))]^{-1} \\ &= \frac{\sigma^2}{\sum_{n=0}^{N-1}(\frac{\partial s[n]}{\partial\tau})^2} \\ &= \frac{\sigma^2}{\sum_{n=0}^{N-1}(\frac{ds(t)}{dt}|_{t=nT_s})^2} \end{aligned} \tag{5.5}$$

where $\mathbf{E}$ is the expectation operation. T_s is assumed to be small enough so that the sum can be approximated by an integral:

$$\text{var}(\hat{\tau}) \geq \frac{\sigma^2}{\frac{1}{T_s}\int_0^{T_{sym}}(\frac{ds(t)}{dt})^2 dt}. \tag{5.6}$$

Taking the sampling period $T_s = \frac{1}{k(2BW)}$ where k is the oversampling ratio and $\sigma^2 = (N_0/2)(2BW)$, then we have

$$\text{var}(\hat{\tau}) \geq \frac{1}{k}\frac{\frac{N_0}{2}}{\int_0^{T_{sym}}(\frac{ds(t)}{dt})^2 dt}. \tag{5.7}$$

Finally, the CRB can be expressed as [37]

$$\text{var}(\hat{\tau}) = \frac{1}{k}\frac{1}{\frac{\varepsilon}{N_0/2}\bar{F^2}} \tag{5.8}$$

where $\varepsilon = \int_0^{T_{sym}} |s(t)|^2 dt$ is the transmitted signal energy. $\bar{F^2}$is the mean square bandwidth of the signal defined as

$$\bar{F^2} = \frac{\int_{-\infty}^{\infty}(2\pi F)^2 |S(F)|^2 dF}{\int_{-\infty}^{\infty}|S(F)|^2 dF} \tag{5.9}$$

where $S(F)$ the Fourier transform of $s(t)$.

It is known that $\varepsilon = \int^{T_{sym}} |s(t)|^2 dt = T_{sym}\int_{-\infty}^{\infty}|S(F)|^2 dF$. For the chirp signal, the transmitted signal energy ε can be further written as $\varepsilon = T_{sym}BWS(F)^2$.

The spectrum $S(F)$ shown in Fig 2.1 is not flat. These ripples increase the complexity of calculation in $\bar{F^2}$ in (5.8). However, it is reasonable to assume $S(F)$ uniformly distributed over the bandwidth since the integral of $S(F)$ is roughly equivalent to the integral of some constant as shown in Fig 5.1. Then $\bar{F^2}$ can be simplified to

$$\bar{F^2} = \frac{4\pi^2(BW)^2}{3}. \tag{5.10}$$

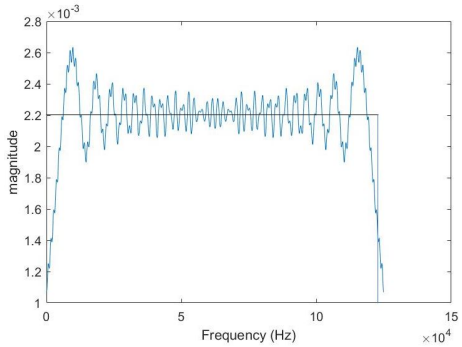

Figure 5.1: Spectrum of transmitted signal with sequential bands

The ratio of signal power to noise is

$$SNR = \frac{P_s}{P_n} = \frac{\varepsilon / T_{sym}}{\frac{N_0}{2} \times (2BW)} \tag{5.11}$$

where P_s and P_n are the signal power and noise power respectively.

Then the CRB in (5.8) can be rewritten as

$$\text{var}(\hat{\tau}) = \frac{3}{8\pi^2 k T_{sym} (BW)^3 SNR} \tag{5.12}$$

and the CRB for range R can be written as $\text{var}(\hat{R}) = c^2 \text{var}(\hat{\tau})$, where c is the speed of light. Note that $k = 1$ when Nyquist sample rate is taken.

Due to the spread spectrum modulation scheme, LoRa devices are able to receive signal powers below the receiver noise floor. The following table shows the mimumum required SNR, and the SNR should be larger than these values to ensure successful reception.

Table 5.1: Required SNR for various modulation configurations

Modulation	SNR
LoRa SF=12	-20 dB
LoRa SF=11	-17.5 dB
LoRa SF=10	-15 dB
LoRa SF=9	-12.5 dB
LoRa SF=8	-10 dB
LoRa SF=7	-7.5 dB

6 Simulation Results

In this section, we conduct the simulations to investigate the performance of the above mentioned three TOA estimation algorithms in single and multipath conditions. The simulation results are obtained through 1000 independent Monte Carlo trials. In the TOA estimation, only the root means square error (RMSE) for the first arrival path is considered. At the receiver, the received LoRa signal is firstly normalized to the unit power, and then AWGN noise with the specified variance is added for Monte-Carlo simulations. MUSIC and ESPRIT mentioned in this chapter refer to FBCM-MUSIC and TLS-ESPRIT.

SNR in dB is defined as $10\log_{10}(P_r/P_n)$, where P_r and P_n are the power of one symbol $c(t)$ and the noise $w(t)$, they are defined in the simulation as $\frac{1}{N}\sum_{n=0}^{n=N-1} r^2[n]$ and $\frac{1}{N}\sum_{n=0}^{n=N-1} w^2[n]$, respectively. The used signal is a chirp symbol sequence with the following parameters:

- Bandwidth = 125kHz,
- Symbol duration = 1ms,
- Number of integration symbols = 8,
- Sampling rate = 1MHz/s,
- Spreading factor = 7.

The wireless channel is modeled as discrete multipath channel. The power delay profile in urban and rural areas is shown in Fig 6.1 and table 6.1 shows related parameters. The probability density of the complex amplitude of delays follows Rayleigh distribution.

Parameters	Outdoor	Outdoor
Environment	Rural NLOS	Urban LOS
Excess Delay Spread	5 μ s	0.5 μ s
Mean Delay Spread	1.09 μ s	0.13 μ s
RMS Delay Spread	1.43 μ s	0.14 μ s

Table 6.1: Characteristics of wireless channel model

The simulation experiment aims to estimate the performance of three algorithms and the efficiency of the multiband architecture. The algorithms will be tested in both single and multipath channel in terms of different SNR values and the number of chirp signals used. The efficiency of the multiband architecture will be investigated.

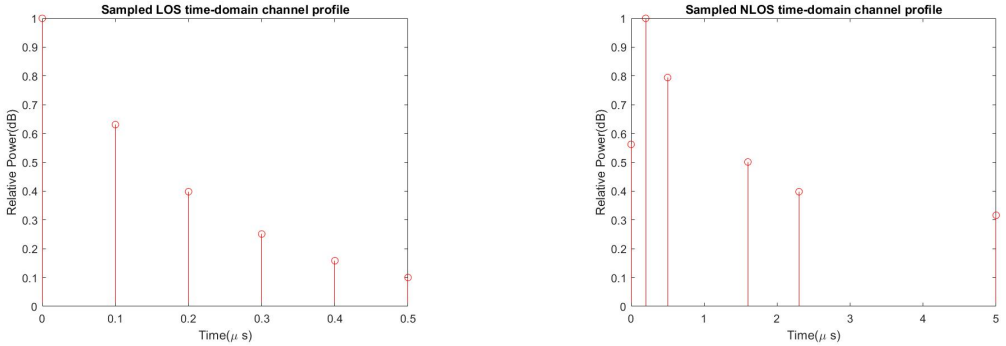

(a) (b)

Figure 6.1: Outdoor power delay profile in a. Rural area (LOS) b. Urban area (NLOS)

6.1 Single Path AWGN Channel

The simulation is conducted in the single path channel to compare the performance of different algorithms with CRLB for LoRa signals. It also compares the impact of 8-symbol structure with the conventional structure which has only one symbol. This experiment is designed to look into the advantage of the LoRa packet structure. Fig 6.2 shows the RMSE of the ranging error of three algorithms as a function of SNR. In an ideal scenario without multipath effect, the RMSE at SNR=-5 decreases from 70m to 25m by using eight symbols instead of one, and the corresponding CRLB is reduced from 30 to 10m. There is an imperceptible difference among the performance of the matched filter, MUISC and ESPRIT in single path channel. The RMSE of the matched filter goes higher than that of the MUSIC and ESPRIT when SNR is larger than 15. One possible reason is that the ranging resolution of the matched filter depends on the sampling rate, so its ranging error could only be certain values.

In some cases, multiple experiment data is required to perform certain algorithms, in other words, the experiment has to be repeated multiple times in exactly the same environment. However, eight identical upchirps in the LoRa preamble dispense with this problem. These eight upchirps can be regarded as eight observations. It is equivalent to one upchirp signal being transmitted eight times within the coherent time. The idea is to average these eight coarse CFR estimates with the same weight, in this way, the AWGN noise is reduced.

The cumulative distribution function (CDF) is used to compare the performance of these algorithms, when SNRs are 1, 7, 13 and 19. Comparing with correlation-based techniques, subspace-based techniques improve the ranging resolution and accuracy at the cost the complexity. However, as shown in Fig 6.3, this advantage only appear at high SNRs, which means these algorithms have to work above certain noise level (e.g. SNR=5) to have a good performance. As we have mentioned above, the ranging error of the matched filter could only be certain values, and it explains the reason why the CDF plot of the matched filter is not as smooth as MUSIC and ESPRIT.

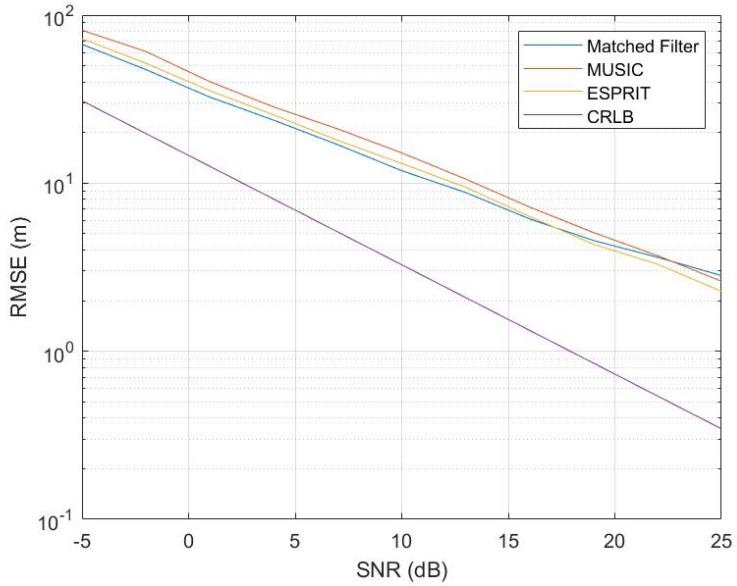

(a)

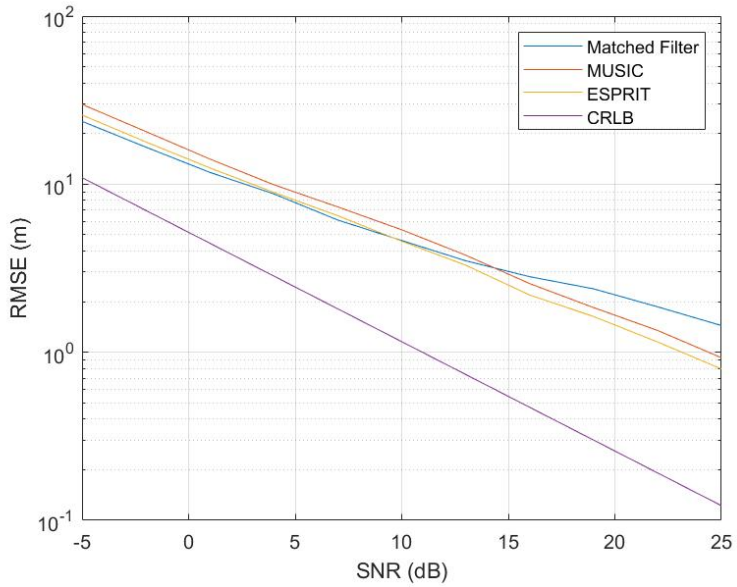

(b)

Figure 6.2: RMSE of absolute ranging errors of different methods in a 1-path channel for (a) one symbol and (b) eight symbols

6.2 LOS and NLOS Multipath Channel

We first implemented the selected algorithms in absence of noise, so that we only observe the impacts of different environment scenarios. Fig 6.4 displays the CDF of TOA estimation errors of these algorithms in both LOS and NLOS 6-path channels

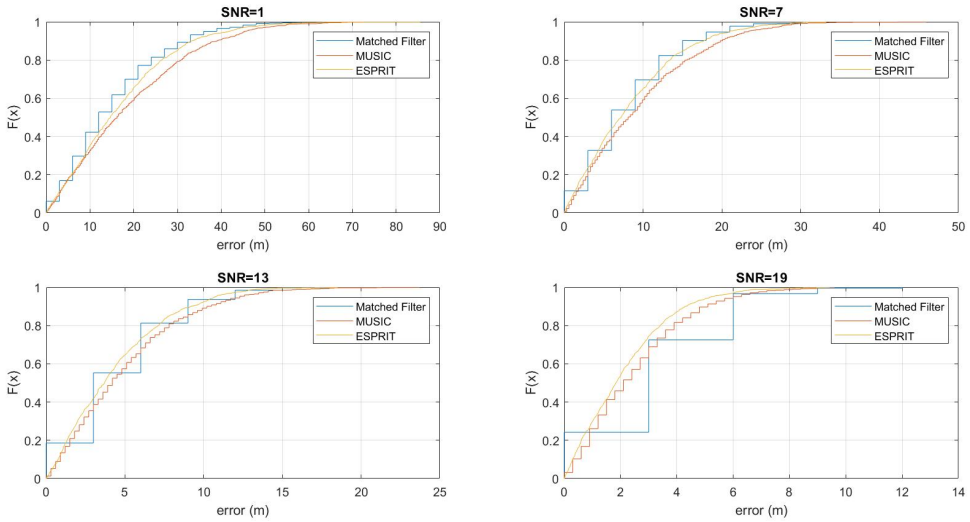

Figure 6.3: CDF of absolute ranging errors in a 1-path channel when SNR = 1, 7, 13 and 19

without noise. In general, the subspace-based techniques outperform the correlation-based techniques in both scenarios as we expected. At the same time, ESPRIT has better performance than MUSIC in terms of the CDF of ranging errors. As we can see in Fig 6.4 (a), 90% ranging errors is less than 26m for ESPRIT and less than 50m for MUSIC in LOS channel. This error of the matched filter is around 5m larger than MUSIC. Fig 6.4 (b) shows the location error in NLOS channel, the 90th percentile errors for the these algorithms in this case increase to 105m, 170m and 740m respectively. The performance of the matched filter deteriorated drastically in NLOS channel than in the LOS channel, because the 90th percentile error increases by around 685m. At the same time, this result also shows the robustness of the subspace-based techniques in different scenarios.

It is evident that the performance of all three algorithms degenerate rapidly in NLOS channel than in LOS channel. According to the simulation results in NLOS scenarios, the performance of subspace-based techniques is better than that of correlation-based TOA estimation methods to different extents. MUSIC and ESPRIT significantly improve the accuracy of localisation when paths are more separated. These simulations indicate that ESPRIT is more accurate compared to MUSIC.

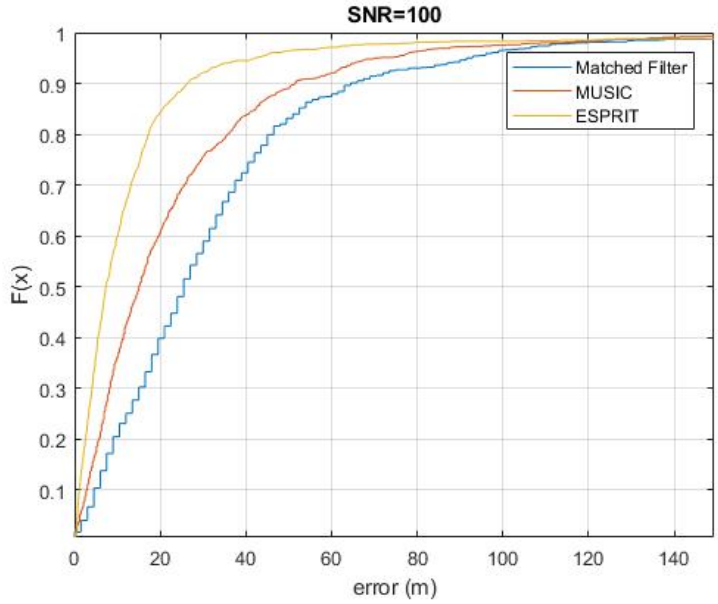

(a)

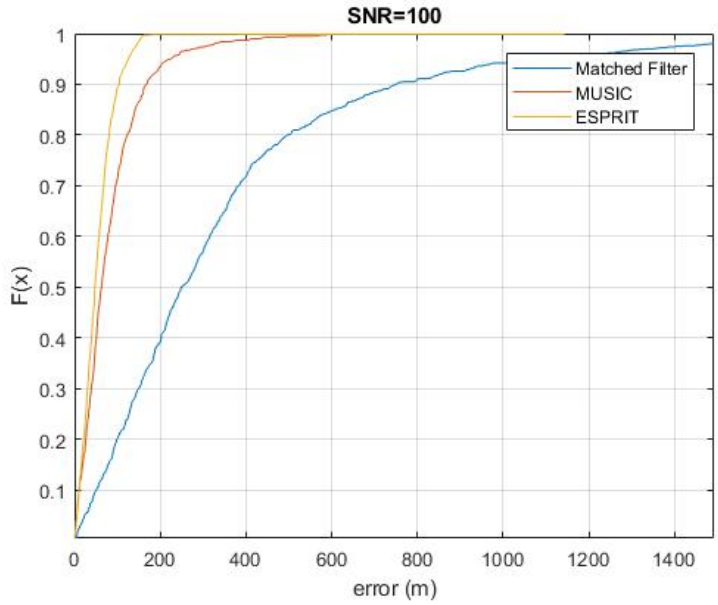

(b)

Figure 6.4: CDF of absolute ranging errors of different methods in (a) LOS and (b) NLOS 6-path channel in absence of noise

6.2.1 LOS Channel

In LOS channel, the strength of the signal from the direct path is higher than that of the other paths. The matched filter estimates the delays by finding the local maxima of the correlation result. So the strength of the path has an influence on the accuracy

for correlation-based techniques. The estimation of subspaced-based technologies like MUSIC and ESPRIT is mainly implemented in the frequency domain. They do not rely on the strength of the path like the matched filter, but will be still affected if the strength difference of from two delays is huge.

Fig 6.5 shows the performance of all algorithms in a 3-path LOS channel. The RMSEs of these three algorithms are still close to each other. At SNR=-5, the RMSE result is around 30m, which is 5m higher than in the single path scenario.

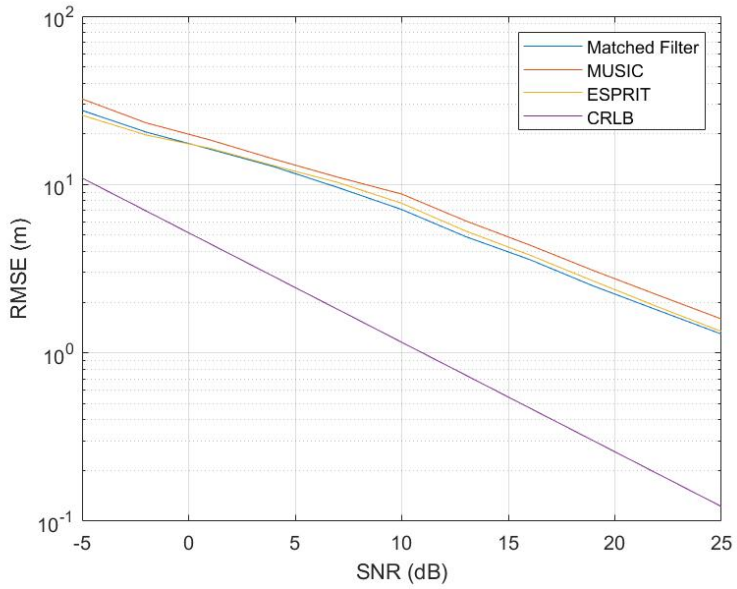

Figure 6.5: RMSE of absolute ranging errors of TOA estimation algorithms in a LOS 3-path channel

The localisation error distribution for 3-path and 6-path channel are shown In Fig 6.6 (a) and (b), respectively. At SNR=20, 90% of this error is less than 50m in 3-path channel and less than around 65m in 6-path channel. In both cases, the 90th percentile error rises by about 15m when SNR reduces from 20 to 0.

It is known that the subspace-based techniques have the ability to resolve closely-spaced paths. Unfortunately, this advantage disappears in all cases shown in the Fig 6.6 since the CDF plots of the three algorithms almost coincide. It is unreasonable to require MUSIC or ESPRIT to resolve two paths with a separation of 30m (0.1μs) with 125kHz bandwidth which already beyond the ability of these subspace-based techniques.

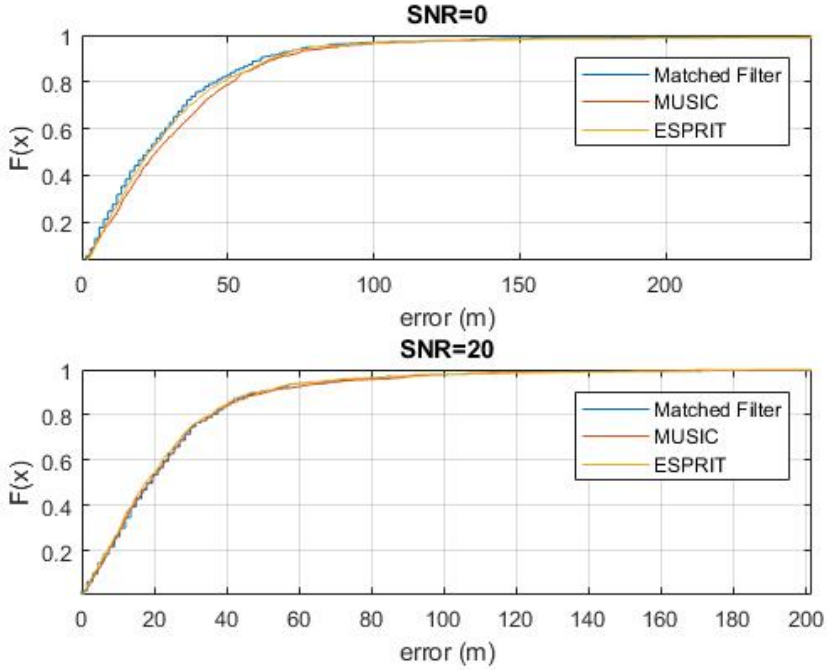

(a)

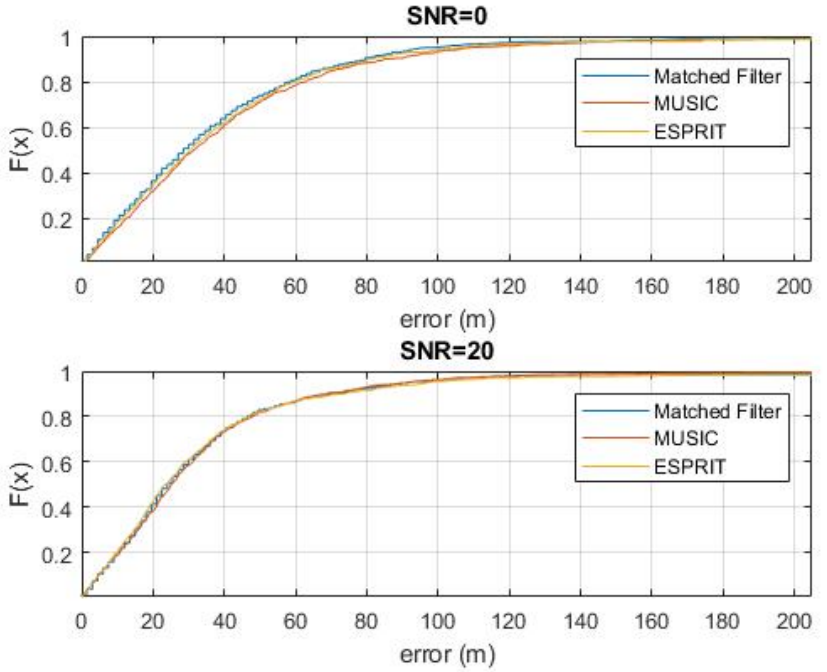

(b)

Figure 6.6: CDF of absolute ranging errors of different methods in (a) 3-path and (b) 6-path LOS channel

6.2.2 NLOS Channel

Unlike the LOS channel, the distribution of time delays in NLOS channel is non-uniform. The difference between two successive delays varies from $\Delta\tau = 0.2\mu$s to $\Delta\tau = 2.7\mu$s. The probability density of the complex amplitude of delays in NLOS channel follows Rayleigh distribution.

In NLOS channel, the second or the third arrival path usually have the strongest energy. As we have discussed above, the TOA estimation of these algorithms depends on the strength of the paths. It is highly likely that the strongest path is taken as the first delay, which would lead to a big estimation error.

Fig 6.7 shows the performance of the selected algorithms in a 3-path NLOS channel and their RMSEs are close to each other. At SNR=-5, the RMSE is around 43m for all algorithms and this error is about 1m when SNR is 25.

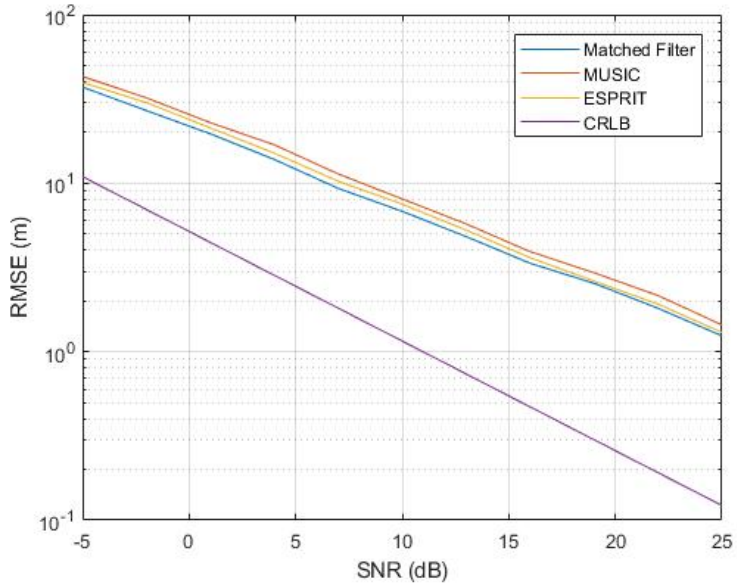

Figure 6.7: RMSE of absolute ranging errors of TOA estimation algorithms in a NLOS 3-path channel

Fig 6.8 studies how the three algorithms behave in both 3-path and 6-path NLOS channel. In Fig 6.8 (a), at SNR=20, 90% localisation error is approximately 150m for these algorithms, and at SNR=0, this error rises to 160m. These three paths are not as closely-spaced as in the LOS scenario, so the 90th percentile error of ESPRIT is 15m lower than that of the matched filter. In Fig 6.8 (b), it is easy to notice that ESPRIT has the best performance at all SNRs. The 90th percentile error is about 285m for ESPRIT, 455m for MUSIC and 710m for the matched filter when SNR is 20. In this case, the accuracy of estimation can be improved by at most 425m by using ESPRIT. While 90th percentile error of the matched filter is around 150m higher than the MUSIC and ESPRIT at SNR=0.

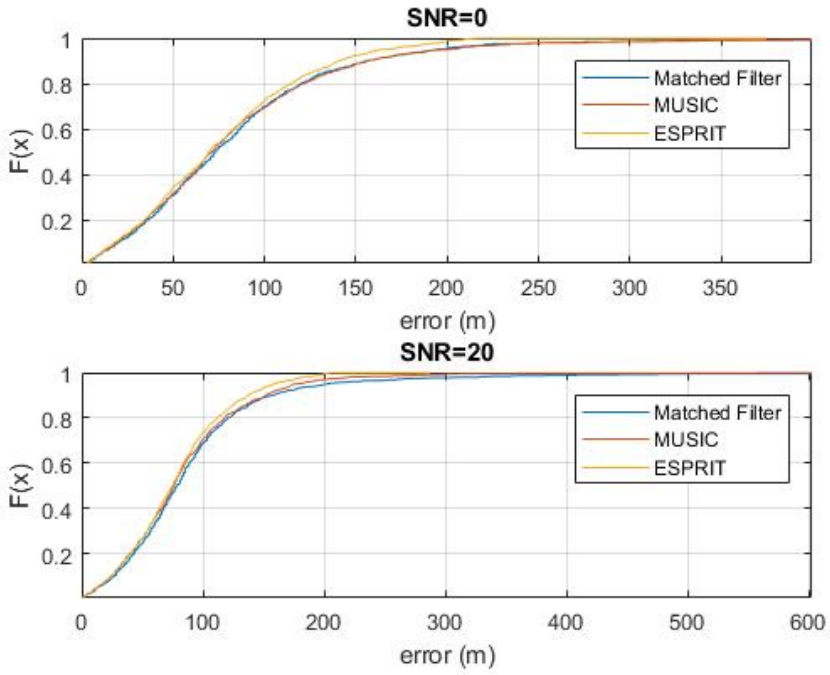

(a)

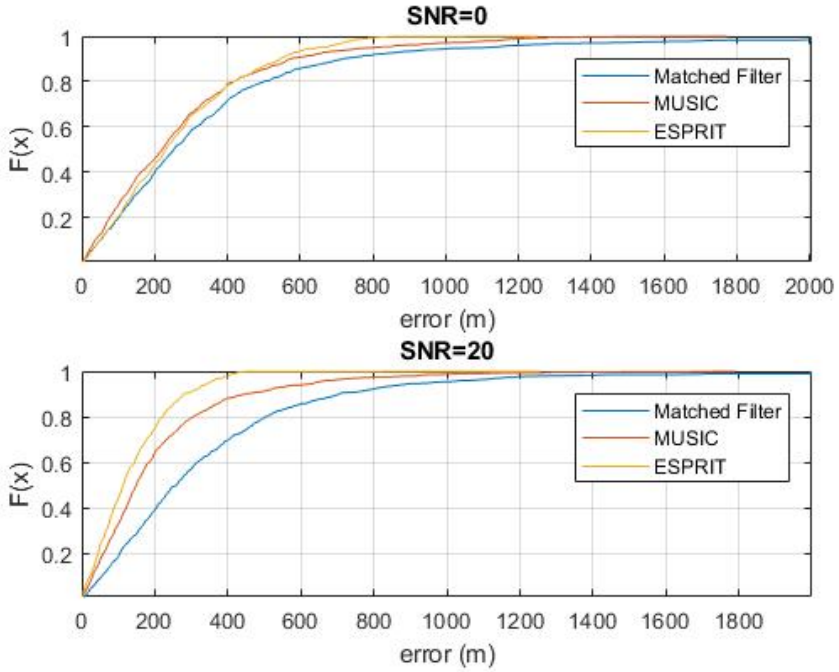

(b)

Figure 6.8: CDF of absolute ranging errors of different methods in (a) 3-path and (b) 6-path NLOS channel

The bandwidth is a major constraint in devising localization approaches based on the channel response. Even for the high-resolution approaches, the bandwidth should be above certain threshold to make them effective. However, the insufficient bandwidth of 125kHz primarily bounds the time resolution and hence those multipath components become indistinguishable. In LOS channels, the separation between two paths is 30m, which is not resolvable for almost all the advanced algorithms. While in NLOS channels, the separation between two paths varies from 60m to 800m, and ESPRIT and MUSIC outperform the matched filter to different extent for different noise levels. Based on the simulation results, it is reasonable to draw the conclusion that subspace-based technologies work better in rural areas than in urban areas. Note that the simulations are done when SF is 7, and the conclusion may be different for higher SF values.

6.3 Noncontiguous Multiband Scenario

In this section, we implemented a multiband scenario with two bands. The performance of the multiband architecture will be compared with the performance using a single band. The parameters are shown below:

- Bandwidth = 125kHz,
- Number of integration symbols = 8,
- Sampling rate = 1MHz/s,
- Number of bands = 2,
- Separation between two bands = 0.3MHz.

In this experiment, the matched filter is implemented in collaboration with the two bands architecture. Fig 6.9 compares the normalized CIR result of the proposed method and from one realisation in the NLOS channel. There is an distinct increase in the resolution of the matched filter in the multiband scenario than in the single-band scenario. Although there is a disconnect between the CFR of two bands, however, we still obtain more useful information of the channel. Fig 6.9 successfully demonstrates the efficacy and efficiency of the proposed multiband architecture. Restricted by the narrow bandwidth, the resolution of the matched filter is too low to detect the multi paths. The matched filter in collaboration with the multiband architecture, not only is a higher resolution achieved, but also an increased accuracy.

In Fig 6.10, the CDF of the proposed method is displayed in comparison with the conventional method in LOS channels. In the graph, two bands are two 125kHz bands with the separation of 300kHz; the single band is 125kHz; and the equivalent band is a single band of 250kHz. It is obvious that the proposed method does not have better performance. It is because the paths are close to each other, the matched filter cannot resolve them even if the bandwidth is doubled or tripled. The time resolution of the matched filter is determined by the bandwidth, which is $c/125\text{K}=2.4\text{Km}$.

In Fig 6.11, the CDF of the proposed method is illustrated in comparison with the conventional method in NLOS channels. At both SNR values, the 90th percentile error

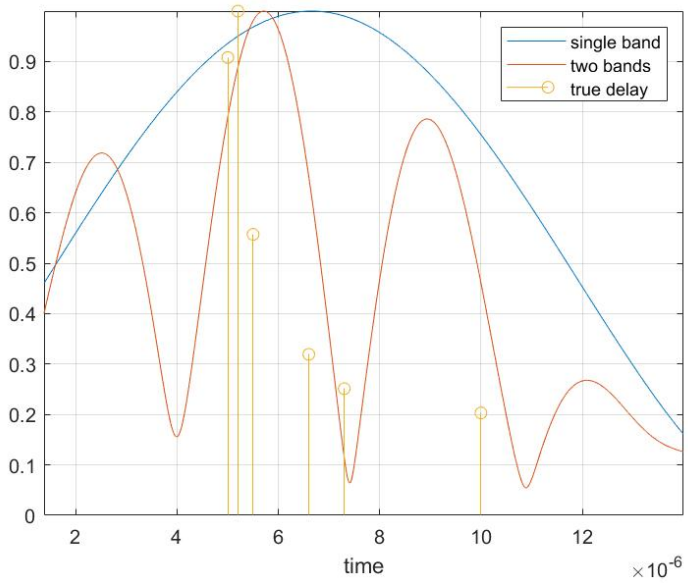

Figure 6.9: Estimated CIR in a two-band scenario

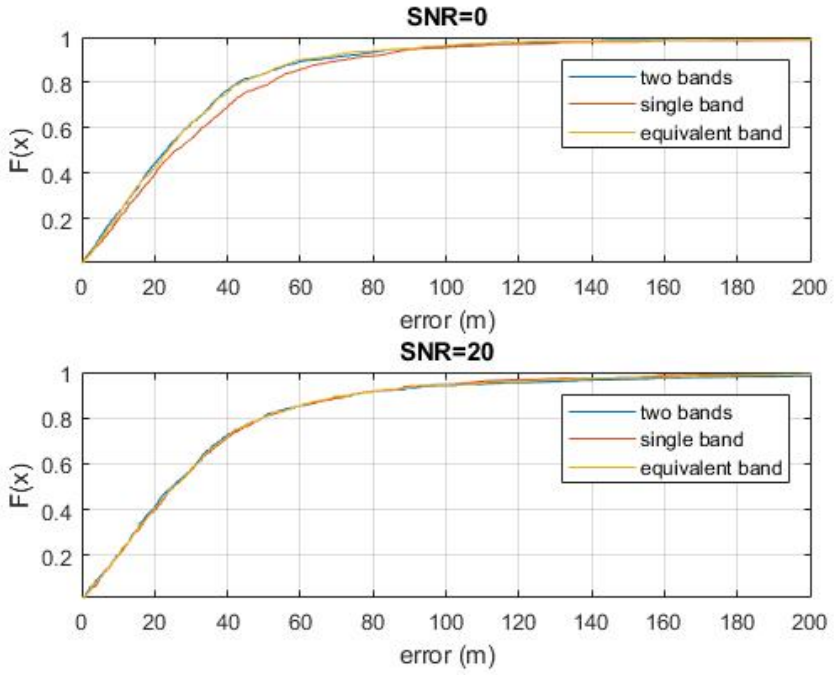

Figure 6.10: CDF of absolute ranging errors of single and multi bands in 6-path LOS channel

is decreased by around 40% by using two bands instead of a single band. Although there is some information missing between two bands, it does not affect the performance of the matched filter. As for the equivalent band, the proposed method still shows better performance and the 90th percentile error is reduced by around 15%. Since two neigh-

boring frequency components have a strong potential for amplitude correlation, and noncontiguous bands will provide more useful and effective information of the channel than the equivalent bandwidth. According to this simulation result, the proposed method improve the accuracy of TOA estimation by about 40% in NLOS channels.

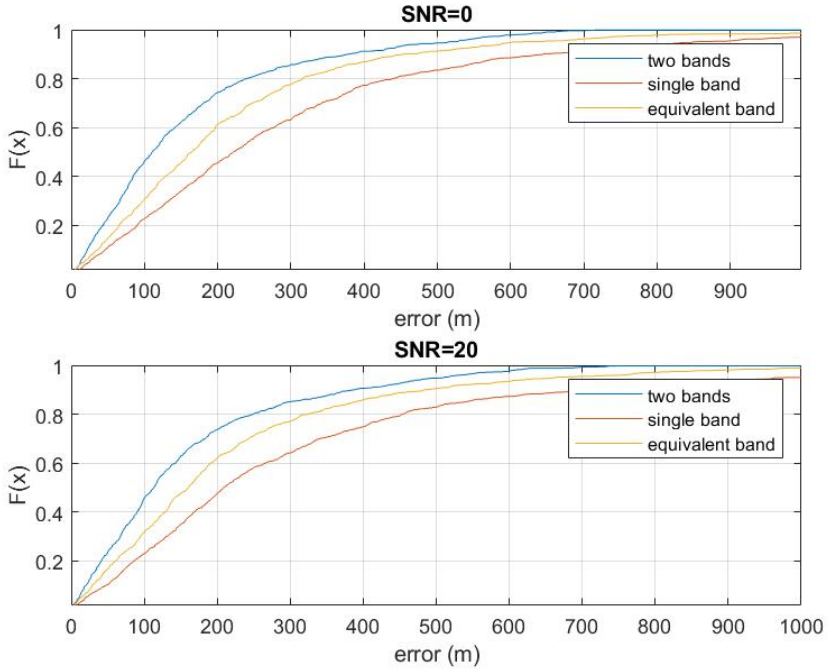

Figure 6.11: CDF of absolute ranging errors of single and multi bands in 6-path NLOS channel

In Fig 6.12, the CDF of the proposed method is illustrated in terms of different separations between the two bands. The differences between two central frequencies f_c are 2.5MHz, 3.0MHz and 3.5MHz, respectively. The performance of these three cases is similar but accuracy is slightly higher when Δf_c is larger.

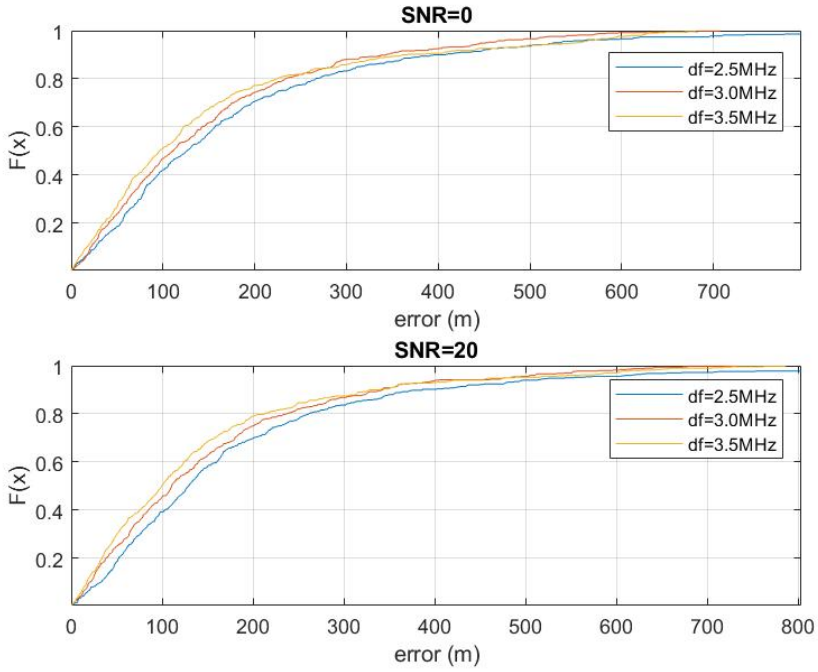

Figure 6.12: CDF of absolute ranging errors of two bands with different differences between central frequencies

6.4 Conclusion

In this chapter, the performance of the matched filter, MUSIC and ESPRIT is presented in three scenarios, and the proposed multiband architecture is studied. First, MUSIC and ESPRIT have similar performance as the matched filter in LOS channel. Because the insufficient bandwidth makes the subspace-based technologies fail to resolve the highly closely-spaced paths. Second, ESPRIT outperforms the matched filter in NLOS channel since it decreases the 90th percentile error by 150m at SNR=0. The reason is that the paths are more far away from each other in this scenario, and the high-resolution approaches are able to show their advantages. Third, the multiband architecture improves the resolution of the matched filter and decreases the 90th percentile error by around 40%.

7 Concluding Remarks

7.1 Conclusions

This thesis aims to improve the ranging accuracy in the outdoor environments using narrow bandwidth LoRa signals. First, CRLB performance in a single path channel is investigated under different sampling rates. Then, three algorithms are implemented for TOA estimation in outdoor environments: the matched filter, FBCM-MUSIC and TLS-ESPRIT. First, the simulations are designed for the no-noise multipath path channel model, and the results show that subspace-based techniques significantly improve the accuracy of TOA estimation as compared with the correlation-based techniques. In the noisy LOS channels, the multi paths are unsolvable for all the three algorithms. Because these paths are too closely-spaced in this scenario, and it is beyond the ability of MUSIC and ESPRIT to distinguish the two paths with a separation of 30m using a bandwidth of 125kHz. The results show that these super-resolution techniques cannot provide better performance than the conventional techniques in rural areas. In the noisy NLOS channels, since the paths are more separated from each other, MUSIC and ESPRIT have better performance than in the LOS channel. Although the paths are resolvable in this scenario, the noise becomes the major constraint on the performance of the super-resolution techniques. Compared to the matched filter, the improvement of MUSIC and ESPRIT in the performance of TOA estimation is less significant at low SNR values. Simulations depict that the multiband architecture is able to decrease the ranging errors by 50% if used properly. Also, it should be noted that the simulations are only for the LoRa signals of SF=7 and BW=125kHz, and these conclusions may not applicable to other SF values and bandwidth.

7.2 Future Works

In this section, some recommendations are presented to extend this research:

- *Testing algorithms on experimental measurements*

  The systems are modelled and tested using MATLAB software. The conclusions are drawn from the simulation results instead of the real experimental data. Since super-resolution techniques show an advantage in NLOS channels, it is vital to check further if this advantage still remain by using real outdoor measurements.

- *Exploiting the frequency correlation properties to expand the bandwidth*

  Coherence bandwidth is the range of frequencies over which two frequency components have a strong potential for amplitude. Then it is possible to estimate the

CFR of the whole coherence bandwidth with the received band and a prior "statistical" knowledge of the channel [38]. It can also be used to estimate the missing information between two sub-bands in the multiband architecture. In the LOS channel model, the rms delay spread is 0.14μs, the coherence bandwidth above 90% correlation is around 140kHz and above 50% correlation is about 1400kHz. While it will never achieve the same accuracy as using the bandwidth equal to this coherence bandwidth.

- *Exploiting the coherent multi-channel ranging for narrowband*

  Multi sub-bands can be applied in different ways where the information of central frequencies of bands are used instead of directly concatenating the CFR of bands. It solves the problem of the phase shift or carrier frequency offset between two bands. However, a two-way transmission is required and it is not applicable to mobile end-devices.

Appendix

A

The results in Fig 6.6 show that MUSIC and ESPRIT cannot provide better performance than the matched filter with a 125kHz bandwidth in the given LOS channel. Now we investigate the minimum bandwidth for MUSIC and ESPRIT to have good performance.

In this appendix, Fig A.1, A.2, A.3 and A.4 show the localisation error distribution of the three algorithms in 6-path LOS channel with higher bandwidth: 0.5MHz, 1MHz, 2MHz and 3MHz, respectively. These figures show that when the bandwidth is higher than 2MHz, MUSIC and ESPRIT are able to provide higher accuracy than the matched filter.

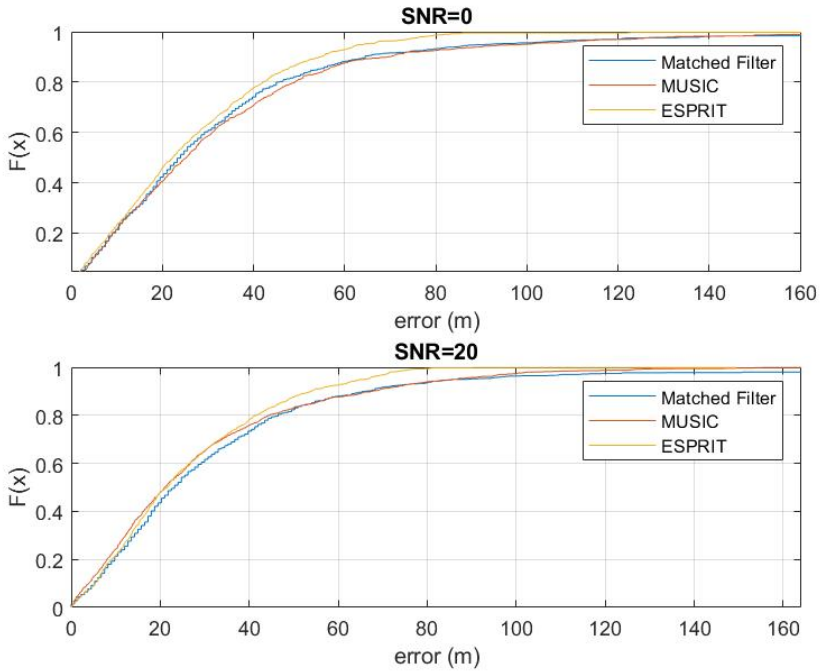

Figure A.1: CDF of absolute ranging errors of different methods in 6-path LOS channels with the bandwidth of 0.5MHz

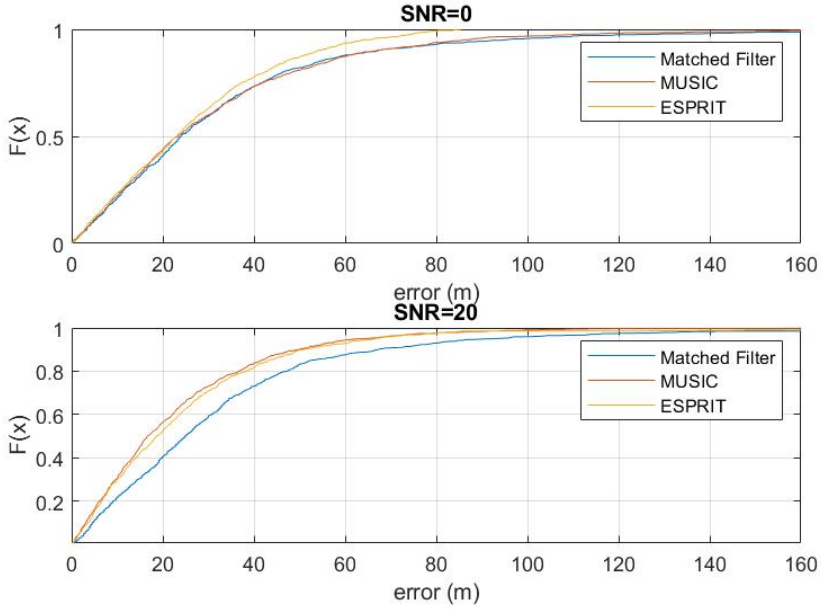

Figure A.2: CDF of absolute ranging errors of different methods in 6-path LOS channels with the bandwidth of 1MHz

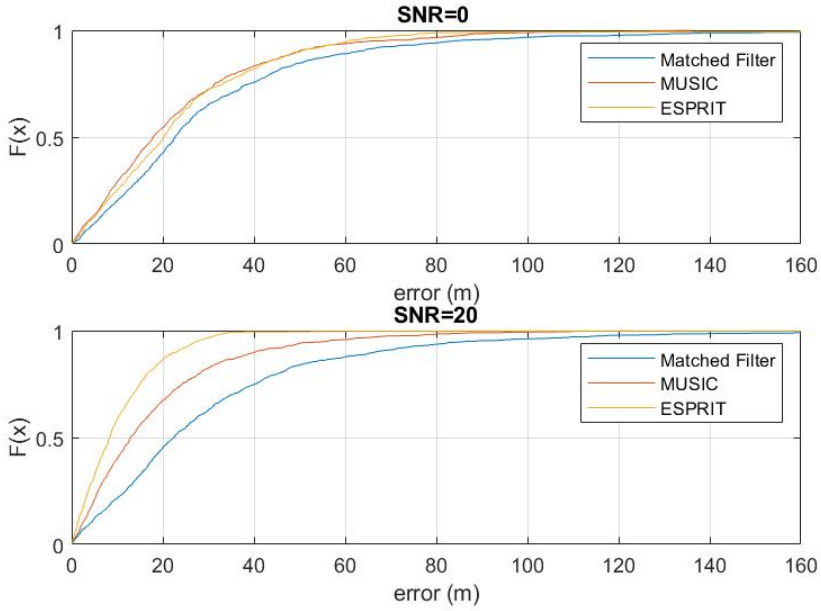

Figure A.3: CDF of absolute ranging errors of different methods in 6-path LOS channels with the bandwidth of 2MHz

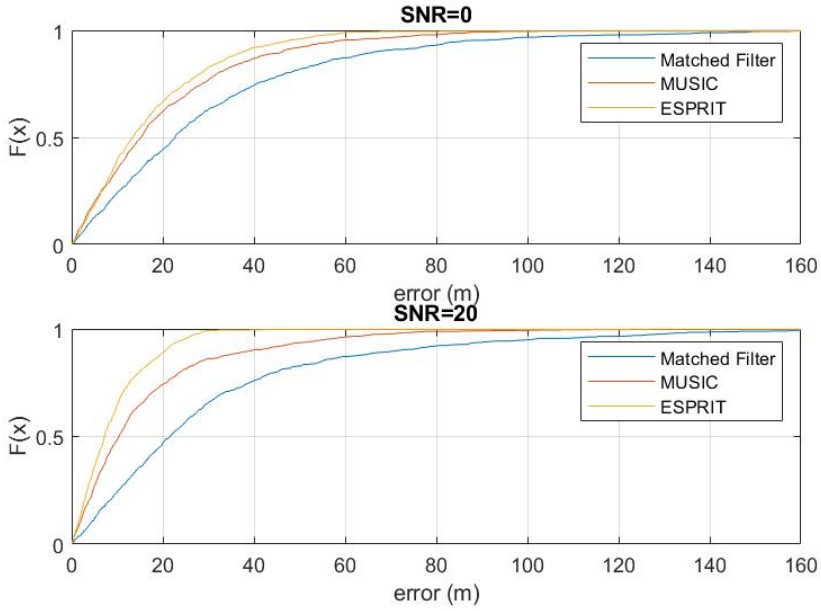

Figure A.4: CDF of absolute ranging errors of different methods in 6-path LOS channels with the bandwidth of 3MHz

Bibliography

[1] "The Future of Internet of Things is at Long Range." [Online]. Available: https://www.loriot.io/LoRawan.html

[2] B. Ray, "What is LoRa? A Technical Breakdown." [Online]. Available: https://www.link-labs.com/blog/what-is-LoRa

[3] A. Augustin, J. Yi, T. H. Clausen, and W. Townsley, "A Study of LoRa: Long Range Low Power Networks for the Internet of Things," *Sensors*, vol. 16, p. 1466, 10 2016.

[4] "LoRa Geolocation," Nov 2017. [Online]. Available: https://gridlocate.com/blog/LoRa-geolocation/

[5] "RF Wireless World." [Online]. Available: http://www.rfwireless-world.com/Terminology/LoRa-modulation-vs-CSS-modulation.html

[6] C. Gu, L. Jiang, and R. Tan, "LoRa-Based Localization: Opportunities and Challenges," 12 2018.

[7] "Understanding the relationship between LoRa chips, chirps, symbols and bits." [Online]. Available: https://electronics.stackexchange.com/questions/278192/understanding-the-relationship-between-LoRa-chips-chirps-symbols-and-bits

[8] L. Vangelista, "Frequency Shift Chirp Modulation: The LoRa Modulation," *IEEE Signal Processing Letters*, vol. 24, no. 12, pp. 1818–1821, Dec 2017.

[9] D. Oh, S. Kim, S. Yoon, and J. Chong, "Two-Dimensional ESPRIT-Like Shift-Invariant TOA Estimation Algorithm Using Multi-Band Chirp Signals Robust to Carrier Frequency Offset," *IEEE Transactions on Wireless Communications*, vol. 12, no. 7, pp. 3130–3139, July 2013.

[10] K. Lam, C. Cheung, and W. Lee, "LoRa-based localization systems for noisy outdoor environment," in *2017 IEEE 13th International Conference on Wireless and Mobile Computing, Networking and Communications (WiMob)*, Oct 2017, pp. 278–284.

[11] ——, "New RSSI-Based LoRa Localization Algorithms for Very Noisy Outdoor Environment," in *2018 IEEE 42nd Annual Computer Software and Applications Conference (COMPSAC)*, vol. 02, July 2018, pp. 794–799.

[12] D. Plets, N. Podevijn, J. Trogh, L. Martens, and W. Joseph, "Experimental Performance Evaluation of Outdoor TDoA and RSS Positioning in a Public LoRa Network," in *2018 International Conference on Indoor Positioning and Indoor Navigation (IPIN)*, Sep. 2018, pp. 1–8.

[13] B. C. Fargas and M. N. Petersen, "GPS-free geolocation using LoRa in low-power WANs," in *2017 Global Internet of Things Summit (GIoTS)*, June 2017, pp. 1–6.

[14] Z. He, Y. Li, L. Pei, and K. O'Keefe, "Enhanced Gaussian Process-Based Localization Using a Low Power Wide Area Network," *IEEE Communications Letters*, vol. 23, no. 1, pp. 164–167, Jan 2019.

[15] D. F. Carvalho, A. Depari, P. Ferrari, A. Flammini, S. Rinaldi, and E. Sisinni, "On the feasibility of mobile sensing and tracking applications based on LPWAN," in *2018 IEEE Sensors Applications Symposium (SAS)*, March 2018, pp. 1–6.

[16] J.-Y. Lee and R. A. Scholtz, "Ranging in a dense multipath environment using an UWB radio link," *IEEE Journal on Selected Areas in Communications*, vol. 20, no. 9, pp. 1677–1683, Dec 2002.

[17] L. Stoica, A. Rabbachin, and I. Oppermann, "A low-complexity noncoherent IR-UWB transceiver architecture with TOA estimation," *IEEE Transactions on Microwave Theory and Techniques*, vol. 54, no. 4, pp. 1637–1646, June 2006.

[18] D. Dardari, C. Chong, and M. Z. Win, "Analysis of threshold-based ToA estimators in UWB channels," in *2006 14th European Signal Processing Conference*, Sept 2006, pp. 1–6.

[19] A. Chehri, P. Fortier, and P. M. Tardif, "Time-of-arrival estimation for IR-UWB systems based on two step energy detection," in *2008 24th Biennial Symposium on Communications*, June 2008, pp. 369–373.

[20] X. Li and K. Pahlavan, "Super-resolution TOA estimation with diversity for indoor geolocation," *IEEE Transactions on Wireless Communications*, vol. 3, no. 1, pp. 224–234, Jan 2004.

[21] T. K. Sarkar and O. Pereira, "Using the matrix pencil method to estimate the parameters of a sum of complex exponentials," *IEEE Antennas and Propagation Magazine*, vol. 37, no. 1, pp. 48–55, Feb 1995.

[22] D. Oh, M. Kwak, and J. Chong, "A Subspace-Based Two-Way Ranging System Using a Chirp Spread Spectrum Modem, Robust to Frequency Offset," *IEEE Transactions on Wireless Communications*, vol. 11, no. 4, pp. 1478–1487, April 2012.

[23] A. Yaqoob, U. Farooq, G. Abbas, and M. U. Asad, "Efficient Hardware Implementation of ESPRIT-like Algorithm for Range Estimation of Chirp Spread Spectrum," *International Journal of Computer and Electrical Engineering*, pp. 473–476, 01 2011.

[24] D. Oh, J. Lee, and J. Chong, "An Effective Pre-Filtering Method with a Propagator for TOA-Based Range Estimation Using Chirp Signal," *IEEE Communications Letters*, vol. 15, no. 9, pp. 929–931, September 2011.

[25] F.-X. Ge, D. Shen, Y. Peng, and V. O. K. Li, "Super-resolution time delay estimation in multipath environments," in *2004 IEEE Wireless Communications and Networking Conference (IEEE Cat. No.04TH8733)*, vol. 2, March 2004, pp. 1121–1126 Vol.2.

[26] K. Yu and E. Dutkiewicz, "NLOS Identification and Mitigation for Mobile Tracking," *IEEE Transactions on Aerospace and Electronic Systems*, vol. 49, no. 3, pp. 1438–1452, July 2013.

[27] C. Ma, R. Klukas, and G. Lachapelle, "A Nonline-of-Sight Error-Mitigation Method for TOA Measurements," *IEEE Transactions on Vehicular Technology*, vol. 56, no. 2, pp. 641–651, March 2007.

[28] F. Wolf, J. Doré, X. Popon, S. d. Rivaz, F. Dehmas, and J. Cances, "Coherent Multi-Channel Ranging for Narrowband LPWAN: Simulation and Experimentation Results," in *2018 15th Workshop on Positioning, Navigation and Communications (WPNC)*, Oct 2018, pp. 1–6.

[29] F. Wolf, C. Villien, S. de Rivaz, F. Dehmas, and J. Cances, "Improved multichannel ranging precision bound for narrowband LPWAN in multipath scenarios," in *2018 IEEE Wireless Communications and Networking Conference (WCNC)*, April 2018, pp. 1–6.

[30] D. G. Manolakis, V. K. Ingle, and S. M. Kogon, *Statistical and adaptive signal processing: spectral estimation, signal modeling, adaptive filtering, and array processing*. Tsinghua University Press, 2003.

[31] "LoRa Frequency Bands in India | LoRa | LoRaWAN - Ensemble Tech," Mar 2018. [Online]. Available: http://www.ensembletech.in/LoRa-frequency-bands-india/

[32] J. Mitola and G. Q. Maguire, "Cognitive radio: making software radios more personal," *IEEE Personal Communications*, vol. 6, no. 4, pp. 13–18, Aug 1999.

[33] M. Pourkhaatoun and S. A. Zekavat, "High-Resolution Low-Complexity Cognitive-Radio-Based Multiband Range Estimation: Concatenated Spectrum vs. Fusion-Based," *IEEE Systems Journal*, vol. 8, no. 1, pp. 83–92, March 2014.

[34] "Duty Cycle," Feb 2019. [Online]. Available: https://www.thethingsnetwork.org/docs/LoRawan/duty-cycle.html

[35] M. Sahmoudi and M. G. Amin, "Fast Iterative Maximum-Likelihood Algorithm (FIMLA) for Multipath Mitigation in the Next Generation of GNSS Receivers," *IEEE Transactions on Wireless Communications*, vol. 7, no. 11, pp. 4362–4374, November 2008.

[36] H. T. Hayvaci, P. Setlur, N. Devroye, and D. Erricolo, "Maximum likelihood time delay estimation and Cramér-Rao bounds for multipath exploitation," in *2012 IEEE Radar Conference*, May 2012, pp. 0764–0768.

[37] Y. Wang, G. Leus, and A. van der Veen, "Cramér-Rao bound for range estimation," in *2009 IEEE International Conference on Acoustics, Speech and Signal Processing*, April 2009, pp. 3301–3304.

[38] Irahhauten, Zoubir and Leus, G and Nikookar, H and Janssen, Gerard, "Uwb ranging based on partial received sub-band signals in dense multipath environments," 06 2010, pp. 1 – 6.